Regionally Correlated Oxygen and Carbon Isotope Zonation in Diagenetic Carbonates of the Bakken Formation

Denny, Adam C.[a*]; Orland, Ian J.[a]; Valley, John. W.[a]

Denny, Adam C.[a*] acdenny@wisc.edu

Orland, Ian J.[a] orland@wisc.edu

Valley, John W.[a] valley@geology.wisc.edu

* Corresponding author

[a.] Department of Geoscience, University of Wisconsin, Madison, WI, 53706 USA

Uploaded Feb. 21, 2020

Final publication:

Denny AC; Orland IJ; Valley JW (2020) Regionally Correlated $\delta^{18}O$ and $\delta^{13}C$ Zonation in Diagenetic Carbonates of the Bakken Formation. Chem. Geol., 531: 1-20. https://doi.org/10.1016/j.chemgeo.2019.119327

Keywords: Bakken, dolomite, burial diagenesis, oxygen stable isotopes, carbon stable isotopes, SIMS

Highlights:

SIMS analyses were made on Devonian-Mississippian middle Bakken member carbonates.

Analyses are from a nine core, ~250 km transect from basin center to margin.

Ankerite-series carbonate growth bands are correlated across the basin by chemistry.

Oxygen and carbon isotopes capture signals of organic maturation and meteoric fluids.

Diagenetic carbonates can preserve >10‰ isotopic variability at the µm scale.

25

26

ABSTRACT

Diagenetic minerals preserve records of burial processes that overprint records of seawater chemistry and impact reservoir porosity. The Mississippian-Devonian aged Bakken Formation in the Williston Basin is a reservoir rock of economic importance whose productivity is affected by diagenetic carbonates, particularly dolomite-ankerite-series carbonates. To investigate how diagenetic carbonate alteration manifests in the Bakken and how that might change across the basin, a combined $\delta^{18}O$ and $\delta^{13}C$ isotope dataset for diagenetic carbonates was collected by in situ SIMS analysis of 10-μm spots from nine drill holes covering a ~250 km transect of the middle Bakken member. Observed core-to-rim isotopic variability in these small Fe-zoned dolomites and calcites frequently exceeds 10‰ in both $\delta^{18}O$ and $\delta^{13}C$, indicating significant changes in thermal and chemical conditions during cementation. Individual ankeritic growth bands can be correlated across the basin by systematic similarities in minor-element compositions and isotope ratios. In the central part of the basin, $\delta^{18}O$ and $\delta^{13}C$ trends at sub-mm-scale decline consistently towards the rims of ankerite-series carbonates, which is interpreted to reflect mineral growth coincident with rising temperatures and an increasing organic contribution to inorganic carbon during burial. The most abrupt shifts in $\delta^{18}O$ and $\delta^{13}C$ (changes as large as 12‰ for $\delta^{18}O$ and 6.5‰ for $\delta^{13}C$ within distances < 15 μm) are observed along the basin margin, and are believed to preserve signals of hydrocarbon expulsion and fluid infiltration along basin margins. Based on the data, we conclude that ankerite-series carbonates preserve records of prolonged thermal and chemical processes that operated basinwide. The isotopic trends presented here show diagenetic rock evolution from shallow dolomite formation to deep burial ankerites, as well as the isotopic responses of carbonates to changing fluids and availability of organic $\delta^{13}C$. These results provide important constraints on how carbonate isotope records may be altered during burial in organic-rich sedimentary rocks and emphasize the need for caution in using bulk powder samples for geochemical analysis in carbonate systems.

1. INTRODUCTION

Diagenetic carbonate cements are μm-scale mineralizations that can grow throughout the burial and lithification of sedimentary rock under low-temperature and low-pressure conditions (Worden and Burley, 2003). Cementation is ubiquitous in sedimentary rocks, and may be influenced chemically (e.g., aragonite recrystallization to calcite, infiltration of meteoric fluids), mechanically (e.g., cements sourced from pressure solution at grain boundaries), or by thermally controlled processes (e.g., organic maturation reactions, clay alteration reactions). Carbonate diagenesis is of interest to the geochemical community due to its potential overprinting of primary seawater isotopic signals (e.g., Banner, 1995; Banner and Hanson, 1990; Barnes et al., 2019; Brand and Veizer, 1981; Kozdon et al., 2011; Irwin et al., 1977; Swart, 2015), impact on permeability and porosity (Brodie et al., 2018; Purser et al., 1994; Sarg, 2012; Sun, 1995), relevance to carbon sequestration (Berger et al., 2009; Bowen et al., 2011), and continued uncertainty of the underlying kinetics and conditions of carbonate, particularly dolomite, formation (Warren, 2000). Understanding the timing and factors that control carbonate diagenesis is important not only for predicting porosity preservation and porosity creation, but also for constraining carbonate behavior during an array of organic and inorganic reactions. Furthermore, understanding how geochemical processes in the subsurface result in the dissolution and precipitation of carbonates is of paramount importance to understanding fluid flow, both for resource development and for optimizing carbon sequestration, where diagenetic reactions are the primary mechanism by which CO_2 will be stored.

Because diagenetic minerals develop under temperature, pressure, and fluid conditions that are commonly present across large areas of basins, it is important that diagenetic studies should attempt to correlate changes in individual μm-scale growth bands laterally through rocks that have experienced different environmental or thermal histories. Secondary Ion Mass Spectrometry (SIMS) is a powerful tool

for reconstructing such diagenetic histories, as it can accurately measure isotopic ratios at the µm scale, and reveal isotopic heterogeneities in minerals that might otherwise be homogenized by more traditional bulk analyses (Cammack et al., 2018; Denny et al., 2017; Harwood et al., 2013; Hyodo et al., 2014; Pollington et al., 2011; Śliwiński et al., 2017a; Teboul et al., 2019).

Presented here are µm-scale diagenetic carbonate $\delta^{18}O$ and $\delta^{13}C$ data of samples collected from a ~250 km transect of the organic-rich, low-porosity middle Bakken member. This study's main goals were: 1) To determine the degree of $\delta^{18}O$ and $\delta^{13}C$ variability preserved at sub-mm-scale in the rock, 2) To determine if carbonate isotopic zonation may be correlated across the basin, and 3) To constrain the formation conditions of early dolomite cements. The results provide insight into how carbonate diagenesis responds to changes in depth, thermal history, and maturity of adjacent petroleum source rocks.

2. GEOLOGICAL BACKGROUND

2.1 Bakken Formation, Middle Member

The Bakken Formation was deposited in the Williston Basin of present-day North Dakota, Montana, and southern Saskatchewan (Fig. 1). It is Devonian-Mississippian in age (Fig. 2a), and is overlain by the Lodgepole Limestone and underlain by the Three Forks Formation (Fig. 2b). The Bakken Formation is divided into a middle, mixed carbonate-siliciclastic member surrounded by upper and lower organic-rich shale members. In the United States the shales have reported average total organic carbon of 8 to 11 weight percent (LeFever et al., 2011; Smith and Bustin, 2000; Sonnenberg, 2011a). The Bakken does not intersect the surface, and all direct study of the formation must be performed using drill core and well logs. It formed in a shallow restricted basin, with the middle Bakken thought to reflect shallower and more oxic conditions than the shales, which were deposited in oxygen-poor conditions (Borcovsky et al., 2017). All three members show a high degree of regional continuity; some authors

argue that individual parasequences within the Bakken may be traced laterally over distances exceeding 150 km (Egenhoff et al., 2011).

In recent years the Bakken Formation has become a prolific source of oil and gas in North America, and there is much resource potential still to be explored—a 2013 assessment by the USGS estimated total unrecovered oil resources to be in excess of seven billion barrels (Gaswirth et al., 2013; Gaswirth and Marra, 2015). The middle member is a significant reservoir for hydrocarbons produced in the adjacent shales despite low porosities ranging from 1 to 11% and an average permeability of 0.0042 mD (Simenson et al., 2011). It is regarded to be an unconventional reservoir, and hydraulic fracturing is used heavily in resource extraction (Sonnenberg et al., 2011b). Carbonate diagenesis had an important impact on present-day porosity, with porous dolomitized zones and fracture distributions contributing significantly to reservoir potential (Pitman et al., 2001; Simenson et al., 2011; Śliwiński et al., 2019).

3. METHODS

3.1 Sample Collection and Preparation

Seventy-four samples were collected from ten drill cores stored at the North Dakota Geological Survey (NDGS) Wilson M. Laird Core and Sample Library. Cores were chosen that intersected the middle Bakken Formation and cover a ~250 km transect from immature source rock conditions along the northeast margin of the basin to mature source rocks in the basin center (Fig. 1). Maximum burial temperatures are estimated to range from ~75 °C on the basin margin sample to ~160 °C in the basin center (Kuhn et al., 2012). All cores and samples were initially described using the lithofacies architecture defined by Egenhoff et al. (2011) (Fig. 2b). Samples were polished and imaged in backscattered electron (BSE) mode using a Hitachi S3400-N scanning electron microscope (SEM) in variable pressure mode; this was found to be the most efficient and effective way of quickly identifying and evaluating the quality of µm-scale ankerite-series zonation. One sample per core was selected to be

prepared for SIMS analysis, as determined by which sample in each core showed the thickest zoned ankerite-series cements in the middle Bakken, and therefore would yield the highest resolution isotopic records by SIMS; one sample, from NDGS core #21706 (not shown in Fig. 1), later proved too friable to produce a good quality polish and was not analyzed further. In preparation for SIMS analysis, 1-2 cm chips were cut from sample rock and cast in Buehler epoxy in 2.54 cm-diameter round molds. In the center of each was mounted the UW-6220 dolomite standard (Valley et al., 2009; Śliwiński et al., 2016a,b). Mounts were then polished to a final grit of 0.25 µm with a diamond suspension and checked for flatness using a reflected light microscope. In total, 11 mounts covering 9 cores were prepared and analyzed by SIMS. To simplify discussion, these cores will hereafter be numbered 1 through 9 (Table 1) from the shallow NE basin margin (core 1) to the deep basin center in the SW (core 9; see Figure 1). Two samples each were prepared in two cores (21668 and 22493) to compare two endmembers of Fe-banded dolomite formation (sandstone dolomites vs. conspicuous fracture or vug dolomites).

3.2 SIMS Procedure

Values of $\delta^{18}O$ and $\delta^{13}C$ were measured on a CAMECA IMS 1280 large-radius, multi-collector secondary ion mass spectrometer (SIMS) at the University of Wisconsin-Madison WiscSIMS laboratory using established sample preparation and analysis procedures (Kita et al., 2009; Valley and Kita, 2009). Samples were analyzed using a focused $^{133}Cs^+$ primary beam with a 10 kV accelerating voltage and 20 keV impact energy. The impact of the $^{133}Cs^+$ atoms sputters ions off of the sample surface and excavates a pit. Pit dimensions were ~11x8 µm for $\delta^{18}O$ analyses and ~9x6 µm for $\delta^{13}C$ analyses; pit depths are estimated to be 2 µm. Charge neutralization is performed with an electron flood gun and a 60 nm gold coat. Sputtered ions are accelerated into a double-focusing mass spectrometer where they are sorted by mass/charge before reaching an array of detectors; $\delta^{18}O$ measurements were made with an array of 3 Faraday cup detectors (for $^{16}O^-$, $^{18}O^-$, and $^{16}O^1H^-$) (Wang et al., 2014) and $\delta^{13}C$ measurements were made using one Faraday cup and two electron multiplier detectors (measuring $^{12}C^-$, $^{13}C^-$, and $^{13}C^1H^-$,

144 respectively). In this study, all SIMS analyses of unknowns were made using dolomite UW-6220 as a
145 running standard (Valley and Kita, 2009), which involves bracketing groups of 8-16 analyses of unknowns
146 with eight analyses on the dolomite standard (4 before the unknowns and 4 after). This bracketing
147 allows users to monitor and correct for small amounts of instrumental drift. Analytical precision for
148 unknowns is typically reported as two standard deviations of the 8 bracketing standard analyses, and is
149 typically ±0.3‰ for $\delta^{18}O$ and ±0.7‰ for $\delta^{13}C$ data reported here (Appendices A, B).

150 The raw isotope ratios obtained by SIMS are affected by an instrumental mass fractionation
151 (IMF) or bias that can vary in magnitude depending on isotopic system, instrumental conditions,
152 mineralogy, and sample composition (Valley and Kita, 2009; Śliwiński et al., 2016a,b, 2017b). IMF is
153 monitored and corrected through the repeated analysis of standards of known composition. It is most
154 sensitive to the concentration of Fe in the carbonate, such that for the conditions of this study, ankerite-
155 series IMFs range by more than 10‰ for $\delta^{18}O$ using 10 µm diameter analysis pits, and may range in
156 excess of 5‰ for $\delta^{13}C$. This effect is particularly pronounced towards dolomitic compositions, where a
157 compositional shift from 0% ankerite (endmember dolomite) to 1.5% ankerite can change the $\delta^{18}O$ IMF
158 by 1.5‰.

159 To address the effect of variable Fe/Mg on analytical IMF, a suite of standards along the
160 ankerite-series are analyzed at the start of each session and used to generate a calibration curve relative
161 to running standard UW-6220 (Śliwiński et al. 2016a,b). After SIMS analysis, this calibration curve is used
162 to determine the composition-specific IMF using an electron microprobe (see EPMA Procedure, below)
163 to determine the Fe concentration (Fe# = Fe/[Fe+Mg]) of each SIMS pit that lies on the ankerite-series.

164 SIMS analyses were monitored for internal error (2SE of individual analyses) or OH or CH ion
165 count rates ($^{16}O^{1}H$ for $\delta^{18}O$ sessions and $^{13}C^{1}H$ for $\delta^{13}C$ sessions) that were significantly above bracketing
166 standard measurements; these analyses were excluded from later discussion of the data. SEM imagery

was also acquired of all SIMS pits, and analyses that were observed to intersect large inclusions or other mineral phases were not included in data discussion. Quartz and calcite data were corrected using standards UWQ-1 quartz (Kelly et al., 2007) and UWC-3 calcite (Kozdon et al., 2009), respectively. All SIMS data are available in Appendices A and B.

3.3 Electron Probe Microanalysis

Chemical compositions for Ca, Mg, Fe, Mn, and Sr were determined by Electron Probe Micro-Analysis (EPMA) for each carbonate SIMS pit using the CAMECA SX-51 in the Cameron Electron Microprobe Lab at the University of Wisconsin-Madison. Data were collected over two analytical sessions with a ~120 second analysis time and a 15 keV, 20 nA beam, which was defocused to a 5 µm diameter in an attempt to minimize sample damage. Data were processed in the Probe for EPMA software (Donovan, 2018), and background correction was performed using the Mean Atomic Number (MAN) procedure (Donovan and Tingle, 1996). As changes over time in measured intensities are common for EPMA measurements in carbonates, particularly for the element Ca, a self-fitted Time Dependent Intensity (TDI) correction was applied for all elements (Donovan, 2018).

As reliable EPMA measurements cannot be obtained from uneven surfaces, it was necessary that measurements be made at least half the EPMA beam diameter from SIMS pits. Previously acquired SEM-BSE imagery was used to aid in targeting EPMA analysis locations along the same compositional growth bands as SIMS analyses, such that EPMA analyses measure areas compositionally equivalent to that of the SIMS analysis pit. SEM-SE (secondary electron) imaging was made of regions post-EPMA as an additional verification that EPMA analyses were properly located, and compared to SEM-BSE imaged zonation to verify that SIMS-equivalent chemistries were obtained. Two to four analyses were made adjacent to each SIMS analysis pit and their chemistries were averaged. If an EPMA analysis was found by SEM imaging to have analyzed a growth band different from the SIMS analysis, or if elemental totals

for an EPMA analysis fell outside of the 98 to 101% range, then it was not included in the calculation of the chemistry at each SIMS analysis.

4. RESULTS

The following sections describe the SIMS data, first concerning the overall trends observable in the data basinwide, and then as it relates to middle Bakken petrography on a sample-specific basis. Readers wishing to see the data broken down in detail should proceed to Section 4.2. All $\delta^{18}O$ data are reported in ‰ VSMOW, and $\delta^{13}C$ data are reported in ‰ VPDB. Equivalent values of $\delta^{18}O$ are provided on the VPDB scale in Appendix A. To simplify discussion, the term "dolomite" will only be used to describe non-ferroan, near-stoichiometric $(Ca,Mg)CO_3$ carbonates (Fe# < ~0.02), whereas carbonates which are on the dolomite-ankerite solid solution and contain iron will be referred to as "ankerite-series carbonates". Unless otherwise noted, ankerite-series Fe contents will be reported as Fe# (mol. Fe/[Fe+Mg]).

4.1 Overview of Mineral $\delta^{18}O$ and $\delta^{13}C$ Data

4.1.2 $\delta^{18}O$ and $\delta^{13}C$ Distributions in Minerals

Banded ankerite-series cements and calcite both show large variability in $\delta^{18}O$ (Fig. 3) and $\delta^{13}C$ (Fig. 4). This variability is often larger than 10‰ across banded carbonates (some < 100 µm wide) and is reproducible from grain to grain within an individual sample. This systematic zonation of ankerite-series cements in $\delta^{18}O$ and $\delta^{13}C$ parallels zonation in Fe#. Because SEM-BSE imaging of Fe-zonation aided in the identification of all growth stages of ankerite-series carbonates in each sample, the ranges of $\delta^{18}O$ and $\delta^{13}C$ present in these histograms reflects the true isotopic range present in each sample at the µm scale. With the exception of the two samples from the margin of the basin (Wells 1 and 2), there is a basin-wide correlation between increasing Fe content, decreasing $\delta^{18}O$, and decreasing $\delta^{13}C$ from core to rim in ankerite-series cements (Fig. 5a). Note that stable isotope variability at this scale could not be

measured by other techniques; data measured by conventional acid dissolution yield average values and do not record distinct burial events.

Calcite also shows large (often >10‰) variability in $\delta^{18}O$ (Fig. 3) and $\delta^{13}C$ (Fig. 4) values, and the range of values for calcite overlaps closely with ankerite-series carbonate ranges in most samples (Fig. 6). Unlike Fe-banded ankerite-series carbonates, SEM imaging of calcite does not readily show compositional zonation at this scale, either by BSE or CL, which makes the selection of analysis spots that represent the full isotopic spectrum of calcite more challenging, especially in fine-grained rocks. Because the growth sequence could not be imaged, calcite was analyzed less often than ankerite-series carbonates (for which Fe-zonation patterns are apparent).

On the whole, quartz overgrowths >10 μm thick appear to be rare in the middle Bakken, although locally-significant diagenetic quartz growth may still occur. Quartz $\delta^{18}O$ values were analyzed in 23 spots from core 3 (Fig. 3c), which contained large and pervasive quartz overgrowths. Classifying all quartz analyses according to whether they were made on detrital grains or overgrowth (as evaluated by SEM-CL imagery) reveals a bimodal distribution, with detrital grains clustering towards $\delta^{18}O$ = 10‰ and overgrowths clustering towards 30‰ (Fig. 7). This bimodality indicates a dominantly high-temperature igneous and metamorphic origin for the detrital quartz grains and low temperatures of cementation for quartz overgrowths. These observations are consistent with previous studies (Denny et al., 2017; Graham et al., 1996; Harwood et al., 2013; Hyodo et al., 2014; Pollington et al., 2011, 2016; Williams et al., 1997). Very little evidence of $\delta^{18}O$ zonation was detected within individual quartz overgrowths, though this is likely in part due to the small width of overgrowths relative to the spot size.

4.1.2 Growth Zones of Ankerite-series Cement

To aid classification and facilitate discussion of analyzed dolomite and ankerite cements, ankerite-series cements are qualitatively divided into 3 growth zones based on a pervasive pattern of

zonation observed repeatedly by SEM-BSE. As schematically illustrated in Figure 8, each successive zone of the cement is delineated by a stepped increase in Fe-content along a traverse from core to rim. Figure 5b and Figure 9 show the distribution of Zones 1, 2, and 3 in plots of $\delta^{18}O$ vs. $\delta^{13}C$.

Zone 1 is defined as the earliest-formed dolomite (Fe# = 0.00) cores that make up the center of most of the ankerite-series cements observed in the middle Bakken. Subsequent generations of carbonate are delineated from the dolomite cores by increases in Fe#. In places, this increase occurs along a non-euhedral boundary that is indicative of dissolution or abrasion, while elsewhere in the same sample other dolomite cores might show euhedral morphologies indicative of formation in place. A comparison of the isotopic values between rounded and euhedral dolomites basinwide demonstrates that morphology is not a predictor of chemistry (Fig. 10).

Zones 2 and 3 surround Zone 1 and have higher Fe#s. Zone 2 is defined here as the first significant relative rise in Fe content. Zone 2 Fe#s typically fall in the 0.02-0.1 range. Zone 3 starts at the second sharp rise in Fe content, and includes the last carbonate rims to grow. The Zone 2 to 3 transition tends to occur when Fe#s approach 0.1, but this changeover may occur at Fe#s as low as 0.05 in shallow samples. Zone 2 commonly contains at least one, and in places two, visible (by SEM-BSE) Fe-poor bands (e.g., Figs. 11a) that may even mark a brief return to dolomitic compositions, but will frequently return to Fe#s more typical of Zone 2 before Zone 3 compositions are encountered.

Other studies have reported isotopic zonation in the Bakken, and the 3 zones discussed here may be correlated to the work of others as follows. We use the Zone 1, 2, and 3 nomenclature of Śliwiński et al. (2019), but their Zone 4 is not always present and has been consolidated here into Zone 3 to simplify discussion. We would correlate our Zones 1 and 2 to the Phase 1 and Phase 2 described by Staruiala et al. (2013); an Fe-rich equivalent to Zone 3 is present in the samples examined by Staruiala et al., but was not thick enough to sample by SIMS.

4.2 Sample-Specific Petrography and Geochemistry

This section will present sample-specific descriptions of the observed petrography and geochemistry for each SIMS mount. Mounts are labeled with a "Core number – depth in feet" nomenclature for accurate comparison with other NDGS core records (that are measured in feet); equivalent depths below the surface in meters are provided with each sample name. Samples are presented in order as they would fall along a NE-SW transect starting at the NE shallow basin margin and working towards the deepest part of the basin in the SW. Grain sizes are described under the Wentworth classification scheme (Wentworth, 1922), using the terms medium silt (16 to 31 μm), coarse silt (31 to 63 μm), very fine sand (63 to 125 μm), and fine sand (125 to 250 μm).

Figures 11 through 15 show petrography, SIMS pit locations and stable isotope values for selected sample regions. These images will be referenced in concert with the following results and discussion. SIMS mount maps were created by integrating SEM-BSE imagery, SIMS analyses, and EPMA data in the QGIS software environment (Linzmeier et al., 2018), and additional images showing the locations and values of all SIMS $\delta^{18}O$ and $\delta^{13}C$ analyses in each mount are available in Appendix C.

4.2.1 Well 1, Sample 24883-3743.4 (1141 m)

The shallowest and northeastern-most sample was collected from a predominantly carbonate grain-supported rock at a depth of 1141 m (3743.4 ft.), and was made into a single SIMS mount (Figs. 3a, 3b, Appendix C1). Both medium to fine sand-sized calcite grains (some ooids) and fine to very fine sand-sized quartz grains are present. Calcite cement is present between most calcite grains. Ankerite-series cements are predominantly found either growing into large uncemented pore spaces in the rock, or growing within a 0.5 to 1 mm wide vertical fracture running through the sample. In hand sample, this fracture is predominantly filled with anhydrite, except in a few places (one of which was incorporated into the mount) where 3-4 mm wide diagenetic pyrites are located within the fracture and appear to

have replaced surrounding carbonates leaving silicate grains largely unaffected (Appendix C1). Calcite $\delta^{18}O$ values range from 20.1 to 29.2‰ (n = 13) and $\delta^{13}C$ ranges from -7.4 to 2.6‰ (n = 13). Ankerite-series $\delta^{18}O$ values range from 19.2 to 38.2% (n = 36) and $\delta^{13}C$ ranges from -8.3 to 4.8‰ (n = 31).

In the banded ankerite-series carbonates, the innermost carbonate core (Zone 1) is dolomite (Fe# = 0.00); $\delta^{18}O$ values range from 24.9 to 27.2‰, and $\delta^{13}C$ values range from -0.3 to 3.7‰ (Figs. 3a, 3b). These dolomite cores are surrounded by a euhedral band of carbonate (Zone 2) with Fe#s in the ~0.02-0.04 range (Fig. 3c), slightly higher $\delta^{18}O$ values showing a range of 26.4-29.9‰, and $\delta^{13}C$ values showing a range of -1.9 to 4.8‰, with $\delta^{13}C$ values declining towards the rim. This band is ringed by a double euhedral band of dolomite (Fe# = 0.00) across which $\delta^{18}O$ values spike (from 24.8 to 38.2) and $\delta^{13}C$ values decline abruptly (from -0.7 to -5.9‰). This is surrounded by a broad Fe-rich band (Zone 3) with a semi-euhedral boundary and increasing Fe content (Fe#s from 0.08 to 0.16), a narrow $\delta^{18}O$ range (30.5 to 31.8‰), and very low $\delta^{13}C$ values (-6.6 to -8.3‰) (Figs. 3d, 3e, 3f). The final, outermost band consists of rapidly rising Fe concentrations (Fe#s from 0.01 to 0.12), with $\delta^{18}O$ steadily increasing from 19.2 to 22.9‰ and $\delta^{13}C$ ranging from -2.1 to -0.8. This final band is thin and truncated in fracture carbonates but broad and correlatable within rock pores, suggesting that it formed coincident with or after the precipitation of anhydrite within the fracture.

4.2.2 Well 2, Sample 20249-6013.4 (1833 m)

This sample was collected from a sandstone intercalated with laminated siltstones at a depth of 1833 m (6013.4 ft.), and was made into two SIMS mounts displaying similar petrography (Appendix C2). Fine to very fine sand-sized quartz and fine sand-sized calcite grains are surrounded by significant volumes of banded ankerite-series carbonate and anhydrite. No fractures or other structural features were observed. Calcite $\delta^{18}O$ ranges from 27.6 to 29.7‰ (n = 6) and $\delta^{13}C$ ranges from -0.7 to 0.8‰ (n = 5). Ankerite-series $\delta^{18}O$ ranges from 23.1 to 35.2‰ (n=63) and $\delta^{13}C$ ranges from -3.2 to 4.0‰ (n = 40).

In the banded ankerite-series carbonates, the innermost carbonate (Zone 1) is dolomite with Fe#s of 0.00, $\delta^{18}O$ values showing a range of 23.1 to 28.2‰, and $\delta^{13}C$ values showing a range of -1.8 to 4.0‰. These dolomite cores commonly show rounded morphologies and internal banding, though others show euhedral morphologies indicative of formation in place. Surrounding the dolomite core is a band of carbonate (Zone 2) with higher Fe#s (~0.04), $\delta^{18}O$ values ranging from 25.0 to 26.3‰, and $\delta^{13}C$ ranging from 0.6 to 4.0‰ (Figs. 12a, 12b). This band is in turn surrounded by a double band of more Fe-poor carbonate (Fe#s 0.02 to 0.03), similar to that in C24883, with $\delta^{18}O$ values spiking from 26.3 up to 35.2‰ (Fig. 12b), and a range of $\delta^{13}C$ values between 0.0 to 3.8‰. This is surrounded by a final region more enriched in Fe (Fe#s 0.05 to 0.10) with $\delta^{18}O$ values ranging from 27.7 to 30.6 and $\delta^{13}C$ ranging from -3.2 to 1.2‰. This final band typically ends in a euhedral rim.

4.2.3 Well 3, Sample 17272-7591.5 (2314 m)

This sample was collected from a sandstone at a depth of 2314 m (7591.5 ft.), and was made into a single SIMS mount (Appendix C3). Fine to very fine sand-sized quartz forms the majority of the grains, but fine to very fine sand-sized calcite grains are also present. Euhedral quartz overgrowths are present around most detrital quartz grains. Banded ankerite-series carbonates are sparse but evenly distributed through the rock, and are large in diameter (> 100 µm). No fractures or other structural features are present. Quartz $\delta^{18}O$ values range from 9.2 to 31.5‰ (n = 22, detrital and overgrowth). Calcite $\delta^{18}O$ values range from 23.2 to 31.3‰ (n = 10) and $\delta^{13}C$ ranges from -4.2 to 5.7‰ (n = 11). Ankerite-series $\delta^{18}O$ values range from 23.4 to 29.8‰ (n = 31) and $\delta^{13}C$ ranges from -7.2 to 2.6‰ (n=30).

In the banded ankerite-series carbonates, the innermost carbonate (Zone 1) is dolomite with Fe#s of 0.00 to 0.01, $\delta^{18}O$ values of 23.7 to 28.1‰, and $\delta^{13}C$ values of -0.8 to 2.2‰. The dolomite cores commonly show rounded morphologies (Figs. 13a, 13c), and some show partial recrystallization and higher Fe#s (up to 0.03). Surrounding these dolomite cores is a band of carbonate (Zone 2) with higher

Fe#s (0.03-0.05), declining $\delta^{18}O$ values from 29.8 to 24.5‰, and declining $\delta^{13}C$ values from 1.1 to -4.5‰. This band is in turn surrounded by a final band of carbonate (Zone 3) with increasing Fe#s from 0.10 to 0.22, $\delta^{18}O$ values in the 23.4 to 25.3‰ range, and rising $\delta^{13}C$ values from -7.2 to -1.9‰ (Figs. 13a, 13d, 13e). This final band possesses a euhedral rim in some locations, but not where it impinges upon calcite grains.

4.2.4 Well 4, Sample 17676-8738.4 (2663 m)

This sample was collected from an isolated ~2-cm thick carbonate-rich shell bed that was isolated in a predominantly sandstone layer intercalated with siltstone at a depth of 2663 m (8738.4 ft.), and was made into a single SIMS mount (Figs. 14a, 14b, Appendix C4). The sample matrix is predominantly composed of microcrystalline calcite and coarse to medium silt-sized ankerite-series carbonates and quartz. Larger banded ankerite-series carbonates have grown in porosity associated with skeletal calcite (Appendix C4). These ankerite-series cements were the main target for SIMS analysis. No fractures or other structural features are present. Quartz $\delta^{18}O$ data range from 16.0 to 27.3‰ (n = 3). Calcite $\delta^{18}O$ values range from 24.5 to 32.1‰ (n = 15) and $\delta^{13}C$ values from -10.3 to 4.8‰ (n = 17). Ankerite-series $\delta^{18}O$ values range from 21.8 to 28.5‰ (n = 32) and $\delta^{13}C$ ranges from -8.8 to 1.4 (n = 37).

In the banded ankerite-series carbonates, the innermost carbonate (Zone 1) is dolomite with Fe#s of 0.00, $\delta^{18}O$ values in the 26.3 to 28.5‰ range, and $\delta^{13}C$ values in the -0.9 to 1.4‰ range. These dolomite cores are euhedral in shape and do not generally show evidence of rounding or recrystallization (Fig. 14a). Surrounding the dolomite cores is a band of carbonate (Zone 2) with higher Fe#s (0.03-0.05), $\delta^{18}O$ values in the 25.8 to 27.3‰ range, and $\delta^{13}C$ values in the -3.7 to -0.9‰ range. This band is in turn surrounded by a final band of carbonate (Zone 3) with increasing Fe#s from 0.10 to 0.15, $\delta^{18}O$ values in the 21.8 to 25.2‰ range, and rising $\delta^{13}C$ values from -8.6 to -4.4‰. This final band possesses a euhedral rim in most locations, but not where it impinges upon skeletal calcites (e.g., 14b).

4.2.5 Well 5, Sample 16586-9812.5 (2991 m)

This sample was collected from a carbonate grain-supported rock from a depth of 2991 m (9812.5 ft.), and was made into a single SIMS mount (Figs. 15a, 15b, Appendix C5). The sample is mainly composed of fine sand-sized calcite grains, with very-fine sand-sized detrital quartz grains being less predominant. Banded ankerite-series carbonates are sparse, but where present tend to be large (100 to 200 µm) when measured from rim to rim. No fractures or other structural features were observed. Calcite $\delta^{18}O$ values range from 24.5 to 28.0 (n = 7) and $\delta^{13}C$ ranges from -2.0 to 5.2‰ (n = 10). Ankerite-series $\delta^{18}O$ values range from 21.7 to 29.5‰ (n = 32) and $\delta^{13}C$ ranges from -5.9 to 3.3‰ (n = 39).

In the banded ankerite-series carbonates, the innermost carbonate (Zone 1) is near to endmember dolomite with Fe#s of 0.01 to 0.02, $\delta^{18}O$ values in the 24.2 to 26.4‰ range, and $\delta^{13}C$ values in the -0.7 to 2.4‰ range. These carbonate cores have a rounded, anhedral contact with subsequent, higher-Fe growth bands, texturally indicative of mechanical abrasion or dissolution. Surrounding these cores is a thin band of carbonate (Zone 2) with higher Fe#s than Zone 1 (~0.06), higher $\delta^{18}O$ values (25.7 to 29.4‰), and heavier $\delta^{13}C$ values (-0.1 to 3.3‰). A thin Fe-poor (Fe#s 0.01 to 0.03) band is next, with $\delta^{18}O$ ~27.0‰ and $\delta^{13}C$ ~-1.1‰. Surrounding this thin Fe-poor band is a broad band with increasing Fe#s (0.05 to 0.09), $\delta^{18}O$ values in the 24.9 to 26.4‰ range, and declining $\delta^{13}C$ values from -0.6 to -4.0‰. Two narrow high-Fe bands follow (Zone 3), the first with Fe#s in the 0.18 to 0.23 range, $\delta^{18}O$ values in the 21.7 to 22.3‰ range, and $\delta^{13}C$ in the -2.9 to -2.9‰ range; the second and final band has Fe#s around 0.38, $\delta^{18}O$ values of ~23‰, and $\delta^{13}C$ values of ~-5‰. These last two Fe-rich bands are not present in many of the sample's banded ankerite-series carbonates (e.g., present in Fig. 15a vs. absent in Fig. 15b), and where they are present they show intermittently anhedral rims suggestive of partial recrystallization to calcite.

4.2.6 Well 6, Sample 17015-10354.4 (3156 m)

This sample was collected from the horizontally laminated siltstone facies at a depth of 2991 m (9812.5 ft.), and was made into a single SIMS mount (Figs. 15c, 15d, Appendix C6). The rock is supported by rounded calcite, quartz, banded ankerite-series carbonate, and feldspar grains in the very fine sand to course silt-size range. Both the feldspars and the ankerite-series carbonate commonly possess euhedral overgrowths; it is difficult to determine based on textural evidence if dolomite was originally grain supporting or if it is replacive after calcite. No fractures or other structural features are present. Quartz $\delta^{18}O$ data range from 10.4 to 17.1‰ (n = 5, detrital and overgrowth). Calcite $\delta^{18}O$ values range from 22.7 to 25.3‰ (n = 17) and $\delta^{13}C$ ranges from -2.2 to 7.5‰ (n = 17). Ankerite-series $\delta^{18}O$ values range from 22.3 to 29.5‰ (n = 47) and $\delta^{13}C$ ranges from -5.5 to 5.1‰ (n = 51).

In the banded ankerite-series carbonates, the innermost carbonate (Zone 1) is near to endmember dolomite; however, while individual near-endmember dolomite cores are homogenous in Fe#, the range of Fe#s varies from grain to grain, from 0.00 to 0.03. These cores also have a wide range of $\delta^{18}O$ values (23.4 to 29.5‰), and $\delta^{13}C$ values in the -2.3 to 3.1‰ range. These carbonate cores commonly show partially anhedral boundaries with surrounding generations, as well as isolated interior pockets containing higher Fe compositions, both of which are typical of partial dissolution/recrystallization textures. Two main bands of different Fe content lie between these cores and the ankerite-series carbonate rim. The first of these (Zone 2) has Fe#s in the 0.06 to 0.12 range, $\delta^{18}O$ values in the 22.6 to 26.6‰ range, and $\delta^{13}C$ values in the -5.2 to 3.9‰ range. The second and final high-Fe band (Zone 3) has Fe#s in the 0.23 to 0.36 range, $\delta^{18}O$ values in the 22.3 to 23.6‰ range, and $\delta^{13}C$ values in the -5.5 to -1.4‰ range. This final band is extremely thin or not present in a portion of the ankerite-series.

4.2.7 Well 7, Sample 21668-10225.8 (3117 m)

This sample was collected from skeletal mudstone at a depth of 3117 m (10225.8 ft.), and was combined with underlying sample C21668-10233.5 into a single SIMS mount (Figs. 15e, 15f, Appendix C7). The rock matrix is dominated by coarse to medium silt-sized silicates and carbonates, and surrounds large (up to 1 cm) skeletal calcites. Skeletal calcite is partially silicified in places, and parts of the sample where skeletal cavities once preserved porosity are now completely infilled with microcrystalline calcite. Grown into one of the larger cavities is a ~1mm diameter fractured banded ankerite-series carbonates, which was the main target for SIMS. Calcite $\delta^{18}O$ values range from 20.4 to 30.8‰ (n = 9) and $\delta^{13}C$ ranges from -6.3 to 6.1‰ (n = 9). Ankerite-series $\delta^{18}O$ values range from 19.3 to 27.7‰ (n = 11) and $\delta^{13}C$ ranges from -8.3 to -0.2‰ (n = 15).

The innermost region of this banded carbonate (Zone 1) is dolomite with an Fe# of 0.00, $\delta^{18}O$ values of 24.6 to 28.0‰, and $\delta^{13}C$ values of -3.1 to -0.3. This is surrounded by a broad band (Zone 2) of more Fe-rich carbonate (Fe#s from 0.04 to 0.10), declining $\delta^{18}O$ values (24.9 to 21.4‰), and $\delta^{13}C$ values in the -7.6 to -3.1‰ range. At this stage of ankerite-series carbonate growth, the mineral was fractured in several places by an unknown mechanism. This fracturing precedes the final, most Fe-rich band (Zone 3, Fe#s of 0.17 to 0.24), which has $\delta^{18}O$ values in the 19.5 to 19.8‰ range and $\delta^{13}C$ values in the -8.2 to -6.7‰ range.

4.2.8 Well 7, Sample 21668-10233.5 (3119 m)

This sample was collected from an oolitic sandstone at a depth of 3119 m (10233.5 ft.), and was combined with overlying sample C21668-10225.8 into a single SIMS mount (Figs. 15g, 15h, 15i, Appendix C7). Rounded calcite grains are medium to fine sand-size, and quartz detrital grains are fine sand to coarse silt- size. Banded ankerite-series carbonates are present throughout. Calcite $\delta^{18}O$ values range from 26.4 to 28.1 (n = 4) and $\delta^{13}C$ ranges from -0.7 to 5.5‰ (n = 4). Ankerite-series $\delta^{18}O$ values range from 22.4 to 30.0‰ (n = 19) and $\delta^{13}C$ ranges from -4.6. to 2.5‰ (n = 16).

The innermost region of this banded carbonate (Zone 1) is dolomite with an Fe# of 0.00, $\delta^{18}O$ values of 23.1 to 30.2‰, and $\delta^{13}C$ values of 0.2 to 2.5‰. Subsequent Fe-compositional zonation in these ankerite-series carbonates is more complex than in other samples. There is a general overall trend of increasing Fe# from core (innermost dolomite) to rim, but in places these banded ankerite-series carbonates also show regions of higher Fe concentration that are not evenly or concentrically distributed about dolomite cores (e.g., Fig. 15i), indicating that they did not form through concentric outward growth of ankerite-series carbonates, and likely result from recrystallization processes. There are two major bins into which Fe#s may be placed. The first (Zone 2) has Fe#s in the range of 0.04-0.08 ($\delta^{18}O$ from 23.0 to 25.2‰ and $\delta^{13}C$ from -3.8 to 0.5‰, and the second (Zone 3) has Fe#s > 0.12 ($\delta^{18}O$ from 22.5 to 23.2‰ and $\delta^{13}C$ from -4.5 to -2.1‰).

4.2.9 Well 8, Sample 12785-11315.5 (3449 m)

This sample was collected from a calcite-filled fracture in a rock with a mixed carbonate-siliciclastic matrix at a depth of 3449 m (11315.5 ft.), and was made into a single SIMS mount (Figs. 15j, 15k, 15l, Appendix C8). The rock matrix is predominantly calcite grains and diagenetic calcite pore-fill, with some detrital quartz; grains are very fine sand-sized. Banded ankerite-series carbonates are sparse in the rock matrix and entirely absent from the fracture itself. Calcite $\delta^{18}O$ values range from 22.9 to 27.0‰ (n=18) and $\delta^{13}C$ ranges from -4.1 to 5.9‰ (n=19). Ankerite-series $\delta^{18}O$ values range from 20.2 to 27.2‰ (n = 20) and $\delta^{13}C$ ranges from -6.1 to 5.2‰ (n = 21).

In the banded ankerite-series carbonates, the innermost carbonate (Zone 1) is dolomite with Fe#s of 0.00, $\delta^{18}O$ values showing a range of 24.9 to 27.2‰, and $\delta^{13}C$ values showing a range of 1.3 to 2.8‰. These dolomite cores show euhedral morphologies. Surrounding many of these dolomite cores is a complex series of bands of carbonate with increasing Fe#s (0.04 up to 0.24), declining $\delta^{18}O$ values (26.2 down to 20.2‰), and fluctuating $\delta^{13}C$ values (-6.1 to 5.2‰) Some of these bands do not appear to

correlate between individual ankerite-series carbonates, and in some cases no Fe-enriched bands are found around the 0.00 Fe# dolomite (e.g., Fig. 15l).

4.2.10 Well 9, Sample 22493-11122.9 (3390 m)

This sample was collected from a sandstone at a depth of 3390 m (11122.9 ft.), and was made into a single SIMS mount (Figs. 15m, 15n, Appendix C9). The rock is supported by detrital quartz, detrital calcite, banded ankerite-series carbonate, and feldspar grains in the very fine sand to coarse silt-size range. Both the feldspars and the ankerite-series carbonates commonly possess overgrowths; it is difficult to determine based on textural evidence if dolomite was originally grain supporting or if it is replacive after calcite. No fractures or other structural features are present. Calcite $\delta^{18}O$ data range from 24.0 to 24.6‰ (n = 3) and $\delta^{13}C$ data range from -2.1 to 1.1‰ (n = 2). Ankerite-series $\delta^{18}O$ values range from 22.3 to 30.4‰ (n = 34) and $\delta^{13}C$ ranges from -5.6 to 5.3‰ (n = 37).

The innermost band in the ankerite-series carbonates (Zone 1) is dolomite with an Fe# of 0.00, $\delta^{18}O$ values of 22.3 to 28.2‰, and $\delta^{13}C$ values in the -0.3 to 4.1‰ range. These dolomite cores commonly show rounded morphologies, and some show partial recrystallization to higher Fe#s (up to 0.18) (e.g., Fig. 15n). Subsequent Fe-compositional zonation in these ankerite-series carbonates is more complex than in other samples, but shares certain textural parallels with C21668-10354.4. There is an overall trend of increasing Fe# from core (innermost dolomite) to rim, but in places these banded ankerite-series carbonates also show regions of higher Fe concentration that are not evenly or concentrically distributed about dolomite cores (e.g., Fig. 15n), suggesting that they did not form through concentric outward growth of ankerite-series carbonates, interpreted to result from recrystallization. There are two major bins into which Fe#s may be placed. The first (Zone 2) has broadly increasing Fe#s in the range of 0.02-0.08 (with declining $\delta^{18}O$ values from 30.3 to 22.8‰ and $\delta^{13}C$ values declining rapidly from 5.3 to -5.6), and the second (Zone 3) has Fe#s > 0.12 (with $\delta^{18}O$ in the 22.4 to 22.9‰ range and $\delta^{13}C$ from -2.1 to -1.0‰).

4.2.11 Well 9, Sample 22493-11159 (3401 m)

This sample was collected from the lower Bakken at a depth of 3401 m (11159 ft.), and was made into a single SIMS mount (Figs. 15o, 15p, Appendix C9). This is the only sample analyzed that was not from the middle Bakken member; the rock was sampled due to the presence of a conspicuous 7 mm-wide fracture bounded by bands of pyrite and containing macroscopic ankerite-series carbonate rhombs. The fracture is in a predominantly calcite rock matrix, with individual crystals in the matrix falling in the 20-50 µm size range. Infilling the fracture is the following growth sequence of minerals: a thin 0.1 mm calcite band, a 0.5 mm band of pyrite, a thick layer of euhedral calcite crystals whose points can stretch 2 mm from tip to base, large fracture-spanning banded ankerite-series carbonate rhombs showing the curved euhedral growth bands typical of 'saddle dolomite' (Radke and Mathis, 1980), and finally, anhydrite filling in the remaining fracture space.

Matrix calcite has $\delta^{18}O$ values ranging 26.5 to 29.5‰ (n = 5) and very negative $\delta^{13}C$ values ranging -17.4 to -12.6‰ (n = 8). Fracture infill calcite shows a $\delta^{18}O$ values in the 23.1 to 26.5‰ range (n = 10), and $\delta^{13}C$ starts low and climbs towards higher values towards the calcite spar tips, from -15.7 up to ~-2‰ (n = 12). Banded ankerite-series carbonates (all Zone 3) show increasing Fe#s as towards the rim (from 0.13 up to 0.30), declining $\delta^{18}O$ values (from 26.6 to 21.9‰, n = 15), and declining $\delta^{13}C$ values (from -1.8 to -10.3‰, n = 25).

5. DISCUSSION

5.1 Dolomite Zone 1

Zone 1 dolomites commonly show rounded boundaries and non-euhedral internal textures that are suggestive of euhedral growth being interrupted by some additional process (e.g., 13c, 15b). Such textures suggest either that rounded dolomites formed from abrasion in a clastic environment on the seafloor, or that a period of dissolution that occurred within the sediment before carbonate

precipitation resumed with ankerite-series compositions. The former interpretation would require dolomite to have formed at or near the sediment-water interface so as to be accessible to mechanical processes on the sea floor. Importantly, not all Zone 1 dolomites within an individual sample show rounded morphologies, indicating that the process was selective and did not affect all grains equally. If there is a mechanism by which heterogeneous dissolution can occur on dolomites at this scale, it is not immediately evident from petrographic observations. Values of $\delta^{18}O$ and $\delta^{13}C$ from Zone 1 show a fair degree of isotopic uniformity if compared between cores across the basin (Figs. 9 and 16a), which could be used to argue for formation from water with nearly constant composition at a narrow range in temperatures, as one would expect if dolomite formed near the sediment-seawater interface.

The range of $\delta^{18}O$ values of dolomite in Zone 1 (most are 24-29‰) presents an interesting interpretational problem, however. If near-surface temperatures (~25 °C) are assumed, the $\delta^{18}O$ of water from which the dolomite precipitated was in the -3 to -8‰ range (Horita, 2014) (Fig. 16a). This is low for marine conditions; estimates for seawater $\delta^{18}O$ at this time are substantially higher at -1.5‰ (Hudson and Anderson, 1989; van Geldern et al., 2006). Three plausible explanations exist for these observations: 1) Basin waters had very low $\delta^{18}O$ values at this time and did not reflect global seawater values, 2) Zone 1 dolomites precipitated from -1.5‰ porewater derived from seawater at around 50 °C, and 3) Petrographic textures reflect early metastable dolomite precipitation near the sediment-seawater interface (25°C) and their isotopic geochemistry was reset when these dolomites recrystallized at higher temperatures.

If the Williston depocenter was sufficiently restricted at this time, it is conceivable that local water may have been driven to lower $\delta^{18}O$ values by meteoric input from either enhanced precipitation or riverine input. Such an interpretation would remove the necessity of invoking elevated temperatures to explain the range of low $\delta^{18}O$ values of these dolomites, and allow for dolomite to form near enough to the surface to allow the grains to be eroded in a clastic environment. However, a variable meteoric

contribution cannot sufficiently explain the sizeable spread of $\delta^{18}O$ and $\delta^{13}C$ values (~5‰) observed in $\delta^{13}C$ and $\delta^{18}O$ measurements of these dolomites *within the same sample*, as such fluids might be expected to be relatively homogenous across these length scales during early dolomite formation.

If, however, precipitation of Zone 1 dolomite occurred from water with a $\delta^{18}O$ value that was no lower than $\delta^{18}O$ = -1.5‰ for the Devonian-Mississippian ocean, then dolomite $\delta^{18}O$ values represent either initial precipitation or recrystallization at higher temperatures of ~50 °C. In the precipitation case, rounded textures would be indicative of dissolution, rather than abrasion, and that dissolution occurred nonuniformly from dolomite grain to dolomite grain. Under this interpretation, the earliest growth phase in these ankerite-series carbonates precipitated at or above 50 °C and no detrital dolomites were present in the Bakken. By contrast, the recrystallization case allows rounded petrographic textures to originate as detrital dolomite, but also necessitates that dolomites recrystallized from metastable precursors at or above 50 °C, resetting their isotope ratios.

With the prevalence of recognizable recrystallization textures in some of the dolomite and ankerite-series carbonates, particularly in the deeper and higher temperature parts of the basin, it is evident that recrystallization has played a role in determining the final isotopic composition of some of these carbonates. Regardless of the origin of rounded dolomite textures, we think that dolomite $\delta^{18}O$ values reflect recrystallization in the soft sediment at ~50°C, a process that has been recognized in other locations (Jones, 2008; Reinhold, 1998). This interpretation is in agreement with fluid inclusion measurements, which indicate that this zone formed below 70°C (Śliwiński et al., 2019).

5.2 Ankerite-series Zones 2 and 3

Zones 2 and 3 formed subsequent to Zone 1 and broadly follow a progression from Zone 1 values towards enriched Fe content and lower $\delta^{18}O$ and $\delta^{13}C$ values (Fig. 5a), and are interpreted as forming along the path towards maximum burial temperatures. Fluid inclusion analyses on early Zone 3

cements from a core along the western basin margin indicate temperatures of formation of ~115-125°C (Śliwiński et al., 2019), which is close to maximum temperatures modeled for that location by Kuhn et al. (2012). Temperature changes have an effect on the dolomite-water fractionation for both $\delta^{18}O$ and $\delta^{13}C$, and the line plotted in Figures 5a and 5b shows the trajectory that a purely temperature-derived isotopic trend will follow if the composition of fluids is constant. The degree of deviation from this line shows that isotopic values in dolomite and ankerite cannot be ascribed solely to changes in temperature, indicating that source pore water $\delta^{18}O$ values increased and/or $\delta^{13}C_{CO2}$ declined over the course of ankerite-series cement precipitation. Thus, ankerite-series cements precipitated over a sufficient period of time to generate changes in temperature and porewater chemistry. The observation that pore water $\delta^{18}O$ increased with time as ankerite-series cements grew is consistent with pore water $\delta^{18}O$ trends observed to occur in other basins in response to water-rock interaction (Clayton et al., 1966). Brines in the middle Bakken today can have $\delta^{18}O$ values in excess of 5‰ (Peterman et al., 2017), and $\delta^{18}O$ in excess of 9.4‰ has been reported for brines from the Devonian Duperow aquifer, which lies below the Bakken (Rostron and Holmden, 2000, 2003).

The progressive trend of dolomite towards lower $\delta^{18}O$ values observed to occur across Zones 2 and 3 is interpreted to be primarily temperature-driven, but temperature effects were partly offset by changing pore water $\delta^{18}O$. Values of $\delta^{13}C$ also decline across Zones 2 and 3, with the lowest $\delta^{13}C$ values generally being associated with the highest Fe#s. This is consistent with increasing interaction of pore waters with low-$\delta^{13}C$ organic matter present in adjacent shales, as CO_2 is produced during the breakdown of organic matter and during hydrocarbon maturation (Surdam et al., 1989). If Zone 3 grew relatively late in the burial history and at near-maximum temperatures, as is suggested by its more ankeritic compositions and low $\delta^{13}C$ values, then one would also expect Zone 3 data to parallel equilibrium fractionation lines for positive $\delta^{18}O_{water}$ values at near maximum burial. Indeed, there is a

progressive trend from Zone 1 to Zone 3 towards equilibrium with a +5 to +10‰ $\delta^{18}O$ basinal brine (Figs. 16b, 16c).

5.3 Late Ankerite in Shallow Cores

Samples collected towards the margin of the basin (Wells 1 and 2) diverge from the above-mentioned trends in some key ways. Fe-poor dolomitic bands present within Zone 2 and correlatable between the two samples are closely associated with high $\delta^{18}O$ values (>30‰). In Well 2 there is no significant correlation of $\delta^{13}C$ with this change in $\delta^{18}O$, but in Well 1 these Fe-poor bands are followed by a thick Fe-rich zone containing $\delta^{18}O$ values ~30‰ and $\delta^{13}C$ values ~-7‰, which require the unusual combination of high $\delta^{18}O$ or low-temperature fluids that have also seen significant conversion of organic to inorganic carbon. The final, Zone 3 growth band in Well 1 contains low $\delta^{18}O$ (~20‰) and $\delta^{13}C$ near 0‰, indicative of high temperature or meteoric fluids that have interacted with carbonates. This last band only appears where porosity is still preserved today, and does not develop any significant thickness in an anhydrite-filled fracture, indicating that it is contemporaneous or post-dates the introduction of anhydrite into the fracture. These isotopic trends necessitate the movement of fluids of significantly different composition from those that precipitated Zone 1 and early Zone 2 ankerite-series carbonates. We propose that the initial ~30‰ band resulted from fluids that migrated out of the deeper parts of the basin during hydrocarbon expulsion, as is known to have occurred along the NE margin of the Williston Basin (Webster, 2011). The final band in Zone 3 must result from low-$\delta^{18}O$ meteoric waters post-expulsion (Fig. 16c), likely associated with hypothesized fresh water influx during the Pleistocene glaciation (Grasby and Betcher, 2000).

5.4 Calcite Cements

Calcite and ankerite-series carbonates show similar magnitudes of variability in both $\delta^{18}O$ (Fig. 3) and $\delta^{13}C$ (Fig. 4). This may indicate that, for some samples (e.g., Well 3), both calcite and ankerite-series

584 carbonate grew or recrystallized under the same range of conditions (Fig. 6). However, not all of the
585 isotope data suggest that diagenetic calcites in the middle Bakken Formation resulted from the same
586 processes as ankerite-series cements. Most of the calcite values in sample 22493-11159 (Well 9) do not
587 parallel the dolomite trend in Fig. 6i. These cements petrographically predate those of the zoned
588 ankerite-series (Appendix C9), and likely resulted from low-temperature methanogenesis in the
589 shallowly buried mud-rich sediments of the lower Bakken member. Indeed, the fracture in sample
590 22493-11159 (Well 9) bears comparison to septarian concretions for its extremely low $\delta^{13}C$ values of
591 both rock matrix and fracture-filling calcites (Siegel et al., 1987; Thyne and Boles, 1989). Despite forming
592 in a shale surrounded by calcites with very negative $\delta^{13}C$ values, the ankerites that have formed within
593 the cracks of the concretion fall along the same trajectory as the other Well 9 sample taken from the
594 middle Bakken. This strongly suggests that the same fluid and temperature trends were driving parallel
595 crystallization of ankerite throughout the formation.

596 # 6. CONCLUSIONS

597 SIMS analyses in zoned carbonates from nine middle Bakken cores demonstrate remarkably
598 large isotopic variability (often > 10‰) for $\delta^{18}O$ and $\delta^{13}C$ on the sub-mm scale, that would otherwise be
599 lost using gas-source mass spectrometry and acid dissolution of bulk powder samples. These zonations
600 are correlatable across a ~250 km transect through the Bakken formation, cover a wide range of burial
601 temperatures, and preserve a history of diagenetic rock evolution from the formation of early dolomites
602 in the shallow sediment on through to deep burial. This indicates that diagenetic processes affecting the
603 middle Bakken carbonates are regional in scope, and that individual growth bands in cements developed
604 in response to diagenetic conditions inherent to the middle Bakken and its neighboring units. Overall
605 trends in ankerite-series minerals strongly indicate a progressive bias of bulk carbonate $\delta^{13}C$ values due
606 to prolonged organic/inorganic mineral interaction. Cements along the basin margin have also recorded

fluid movements into and out of the basin, associated with hydrocarbon expulsion and meteoric water infiltration. Carbonate minerals are sometimes assumed to control the isotope ratio in diagenetic fluids in the subsurface, but the large isotopic variability present in diagenetic carbonates at the micron scale in these samples demonstrates that such rock control cannot be taken for granted in bulk isotopic studies, especially if grain-boundary ion diffusion rates are sufficiently high and carbonate reprecipitation rates are sufficiently low.

ACKNOWLEDGMENTS

The authors thank Maciej Śliwiński for assistance with sample preparation and many insightful conversations, Kouki Kitajima, Noriko Kita, and Mike Spicuzza of the WiscSIMS lab for analytical and instrumental support, John Fournelle for assistance with EPMA; Bil Schneider for SEM support, Brian Hess for sample prep assistance, and the staff at the North Dakota Geological Survey for facilitating easy access to drill core and digital resources. This work is supported by the U.S. Department of Energy, Office of Science, Office of Basic Energy Sciences (Geosciences) under Award Number DE-FG02-93ER14389. WiscSIMS is supported by the U.S. National Science Foundation (EAR-1658823) and the University of Wisconsin- Madison.

APPENDICES

Appendix A – Condensed SIMS dataset

Appendix B – Full SIMS datasets w/ standards and IMF corrections

Appendix C – Mount maps of SIMS data

REFERENCES

Banner, J.L., 1995. Application of the trace element and isotope geochemistry of strontium to studies of carbonate diagenesis. Sedimentology 42, 805–824.

Banner, J.L., Hanson, G.N., 1990. Calculation of simultaneous isotopic and trace element variations during water-rock interaction with applications to carbonate diagenesis. Geochimica et Cosmochimica Acta 54, 3123–3137. https://doi.org/10.1016/0016-7037(90)90128-8

Barnes, B.D., Husson, J.M., Peters, S.E., 2019. Authigenic Carbonate Burial in the Late Devonian–Early Mississippian Bakken Formation (Williston Basin, USA). Sedimentology, accepted.

Berger, P.M., Roy, W.R., Mehnert, E., 2009. Geochemical Modeling of Carbon Sequestration, MMV, and EOR in the Illinois Basin. Energy Procedia 1, 3437–3444.

Borcovsky, D., Egenhoff, S., Fishman, N., Maletz, J., Boelhke, A., Lowers, H., 2017. Sedimentology, facies architecture, and sequence stratigraphy of a Mississippian black mudstone succession—The upper member of the Bakken Formation, North Dakota, United States. American Association of Petroleum Geologists Bulletin 101, 1625–1673. https://doi.org/10.1306/01111715183

Bowen, B.B., Ochoa, R.I., Wilkens, N.D., Brophy, J., Lovell, T.R., Fischietto, N., Medina, C.R., Rupp, J.A., 2011. Depositional and diagenetic variability within the Cambrian Mount Simon Sandstone: Implications for carbon dioxide sequestration. Environmental Geosciences 18, 69–89.

Brand, U., Veizer, J., 1981. Chemical diagenesis of a multicomponent carbonate system; 2, Stable isotopes. Journal of Sedimentary Research 51, 987–997.

Brodie, M.W., Aplin, A.C., Hart, B., Orland, I.J., Valley, J.W., Boyce, A.J., 2018. Oxygen Isotope Microanalysis by Secondary Ion Mass Spectrometry Suggests Continuous 300-million-year History of Calcite Cementation and Dolomitization in the Devonian Bakken Formation. Journal of Sedimentary Research 88, 91–104. https://doi.org/10.2110/jsr.2018.1

Cammack, J.N., Spicuzza, M.J., Cavosie, A.J., Van Kranendonk, M.J., Hickman, A.H., Kozdon, R., Orland, I.J., Kitajima, K., Valley, J.W., 2018. SIMS microanalysis of the Strelley Pool Formation cherts and the implications for the secular-temporal oxygen-isotope trend of cherts. Precambrian Research 304, 125–139. https://doi.org/10.1016/j.precamres.2017.11.005

Clayton, R.N., Friedman, I., Graf, D.L., Mayeda, T.K., Meents, W.F., Shimp, N.F., 1966. The Origin of Saline Formation Waters: 1. Isotopic Composition. Journal of Geophysical Research 71, 3869–3882.

Denny, A.C., Kozdon, R., Kitajima, K., Valley, J.W., 2017. Isotopically zoned carbonate cements in Early Paleozoic sandstones of the Illinois Basin: $\delta^{18}O$ and $\delta^{13}C$ records of burial and fluid flow. Sedimentary Geology 361, 93–110. https://doi.org/10.1016/j.sedgeo.2017.09.004

Donovan, J.J., 2018. Probe for EPMA User's Guide and Reference Manual.

Donovan, J.J., Tingle, T.N., 1996. An improved mean atomic number background correction for quantitative microanalysis. Microscopy and Microanalysis 2, 1–7.

Egenhoff, S., Dolah, A.V., Jaffri, A., Maletz, J., 2011. Chapter 2: Facies Architecture and Sequence Stratigraphy of the Middle Bakken Member, North Dakota, in: Robinson, J.W., LeFever, J.A., Gaswirth, S.B. (Eds.), The Bakken–Three Forks Petroleum System in the Williston Basin. Rocky Mountain Association of Geologists, Denver, Colorado, pp. 27–47.

Gaswirth, S.B., Marra, K.R., 2015. U.S. Geological Survey 2013 assessment of undiscovered resources in the Bakken and Three Forks Formations of the U.S. Williston Basin Province. American Association of Petroleum Geologists Bulletin 99, 639–660. https://doi.org/10.1306/08131414051

Gaswirth, S.B., Marra, K.R., Cook, T.A., Charpentier, R.R., Gautier, D.L., Higley, D.K., Klett, T.R., Lewan, M.D., Lillis, P.G., Schenk, C.J., 2013. Assessment of Undiscovered Oil resources in the Bakken and Three Forks Formations, Williston Basin Province, Montana, North Dakota, and South Dakota, 2013 (USGS Fact Sheet No. 2013–3013).

674 Grasby, S.E., Betcher, R., 2000. Pleistocene recharge and flow reversal in the Williston basin, central
675 North America. Journal of Geochemical Exploration 69–70, 403–407.
676 https://doi.org/10.1016/S0375-6742(00)00092-3

677 Harwood, J., Aplin, A.C., Fialips, C.I., Iliffe, J.E., Kozdon, R., Ushikubo, T., Valley, J.W., 2013. Quartz
678 cementation history of sandstones revealed by high-resolution SIMS oxygen isotope analysis.
679 Journal of Sedimentary Research 83, 522–530.

680 Horita, J., 2014. Oxygen and carbon isotope fractionation in the system dolomite–water–CO_2 to elevated
681 temperatures. Geochimica et Cosmochimica Acta 129, 111–124.
682 https://doi.org/10.1016/j.gca.2013.12.027

683 Huberty, J.M., Kita, N.T., Kozdon, R., Heck, P.R., Fournelle, J.H., Spicuzza, M.J., Xu, H., Valley, J.W., 2010.
684 Crystal orientation effects in $\delta^{18}O$ for magnetite and hematite by SIMS. Chemical Geology 276,
685 269–283. https://doi.org/10.1016/j.chemgeo.2010.06.012

686 Hudson, J.D., Anderson, T.F., 1989. Ocean temperatures and isotopic compositions through time. Earth
687 and Environmental Science Transactions of The Royal Society of Edinburgh 80, 183–192.
688 https://doi.org/10.1017/S0263593300028625

689 Hyodo, A., Kozdon, R., Pollington, A.D., Valley, J.W., 2014. Evolution of quartz cementation and burial
690 history of the Eau Claire Formation based on in situ oxygen isotope analysis of quartz
691 overgrowths. Chemical Geology 384, 168–180. https://doi.org/10.1016/j.chemgeo.2014.06.021

692 Irwin, H., Curtis, C., Coleman, M., 1977. Isotopic evidence for source of diagenetic carbonates formed
693 during burial of organic-rich sediments. Nature 269, 209–213.

694 Jones, B., 2007. Inside-Out Dolomite. Journal of Sedimentary Research 77, 539–551.
695 https://doi.org/10.2110/jsr.2007.056

Kelly, J.L., Fu, B., Kita, N.T., Valley, J.W., 2007. Optically continuous silcrete quartz cements of the St. Peter Sandstone: High precision oxygen isotope analysis by ion microprobe. Geochimica et Cosmochimica Acta 71, 3812–3832.

Kita, N.T., Ushikubo, T., Fu, B., Valley, J.W., 2009. High precision SIMS oxygen isotope analysis and the effect of sample topography. Chemical Geology 264, 43–57. https://doi.org/10.1016/j.chemgeo.2009.02.012

Kozdon, R., Kelly, D.C., Kita, N.T., Fournelle, J.H., Valley, J.W., 2011. Planktonic foraminiferal oxygen isotope analysis by ion microprobe technique suggests warm tropical sea surface temperatures during the Early Paleogene. Paleoceanography 26.

Kozdon, R., Ushikubo, T., Kita, N.T., Spicuzza, M., Valley, J.W., 2009. Intratest oxygen isotope variability in the planktonic foraminifer N. pachyderma: Real vs. apparent vital effects by ion microprobe. Chemical Geology 258, 327–337.

Kuhn, P.P., di Primio, R., Hill, R., Lawrence, J.R., Horsfield, B., 2012. Three-dimensional modeling study of the low-permeability petroleum system of the Bakken Formation. American Association of Petroleum Geologists Bulletin 96, 1867–1897. https://doi.org/10.1306/03261211063

LeFever, J.A., Fever, R.D.L., Nordeng, S.H., 2011. Chapter 1: Revised Nomenclature for the Bakken Formation (Mississippian-Devonian), North Dakota, in: Robinson, J.W., Lefever, J.A., Gaswirth, S.B. (Eds.), The Bakken–Three Forks Petroleum System in the Williston Basin. Rocky Mountain Association of Geologists, Denver, Colorado, pp. 11–26.

Linzmeier, B.J., Kitajima, K., Denny, A.C., Cammack, J.N., 2018. Making maps on a micrometer scale. Eos 99, 24–28.

Peterman, Z., Thamke, J.N., Futa, K., Oliver, T.A., 2017. Characterization and origin of brines from the Bakken-Three Forks petroleum system in the Williston Basin, USA. Mountain Geologist 54, 203–221.

Pitman, J.K., Price, L.C., LeFever, J.A., 2001. Diagenesis and fracture development in the Bakken Formation, Williston Basin: Implications for reservoir quality in the middle member (No. 1653), U.S. Geological Survey Professional Paper.

Pollington, A.D., Kozdon, R., Anovitz, L.M., Georg, R.B., Spicuzza, M.J., Valley, J.W., 2016. Experimental calibration of silicon and oxygen isotope fractionation between quartz and water at 250°C by in situ microanalysis of experimental products and application to natural samples. Chemical Geology 421: 127-142

Pollington, A.D., Kozdon, R., Valley, J.W., 2011. Evolution of quartz cementation during burial of the Cambrian Mount Simon Sandstone, Illinois Basin: In situ microanalysis of $\delta^{18}O$. Geology 39, 1119–1122.

Purser, B.H., Brown, A., Aissaoui, D.M., 1994. Nature, Origins and Evolution of Porosity in Dolomites, in: Purser, B., Tucker, M., Zenger, D. (Eds.), Dolomites. Blackwell Publishing Ltd., pp. 281–308.

Radke, B.M., Mathis, R.L., 1980. On the Formation and Occurrence of Saddle Dolomite. Journal of Sedimentary Research 50, 1149–1168.

Reinhold, C., 1998. Multiple episodes of dolomitization and dolomite recrystallization during shallow burial in Upper Jurassic shelf carbonates: eastern Swabian Alb, southern Germany. Sedimentary Geology 121, 71–95. https://doi.org/10.1016/S0037-0738(98)00077-3

Rostron, B.J., Holmden, C., 2003. Regional variations in oxygen isotopic compositions in the Yeomanand Duperow aquifers, Williston basin (Canada-USA). Journal of Geochemical Exploration, Proceedings of Geofluids Fourth International Conference on Fluid Evolution, Migration and Interaction in Sedimentary Basins and Orogenic Belts 78–79, 337–341. https://doi.org/10.1016/S0375-6742(03)00086-4

742 Rostron, B.J., Holmden, C., 2000. Fingerprinting formation-waters using stable isotopes, Midale Area,
743 Williston Basin, Canada. Journal of Geochemical Exploration 69–70, 219–223.
744 https://doi.org/10.1016/S0375-6742(00)00024-8

745 Siegel, D.I., Chamberlain, S.C., Dossert, W.P., 1987. The isotopic and chemical evolution of mineralization
746 in septarian concretions: Evidence for episodic paleohydrogeologic methanogenesis. Geological
747 Society of America Bulletin 99, 385–394. https://doi.org/10.1130/0016-
748 7606(1987)99<385:TIACEO>2.0.CO;2

749 Simenson, A.L., Sonnenberg, S.A., Cluff, R.M., 2011. Chapter 3: Depositional Facies and Petrophysical
750 Analysis of the Bakken Formation, Parshall Field and Surrounding Area, Mountrail County, North
751 Dakota, in: Robinson, J.W., LeFever, J.A., Gaswirth, S.B. (Eds.), The Bakken–Three Forks
752 Petroleum System in the Williston Basin. Rocky Mountain Association of Geologists, Denver,
753 Colorado, pp. 48–101.

754 Śliwiński, M.G., Kitajima, K., Kozdon, R., Spicuzza, M.J., Denny, A., Valley, J.W., 2017a. In situ $\delta^{13}C$ and
755 $\delta^{18}O$ microanalysis by SIMS: A method for characterizing the carbonate components of natural
756 and engineered CO_2-reservoirs. International Journal of Greenhouse Gas Control 57, 116–133.
757 https://doi.org/10.1016/j.ijggc.2016.12.013

758 Śliwiński, M.G., Kitajima, K., Kozdon, R., Spicuzza, M.J., Fournelle, J.H., Denny, A.C., Valley, J.W., 2016a.
759 Secondary Ion Mass Spectrometry Bias on Isotope Ratios in Dolomite–Ankerite, Part I: $\delta^{18}O$
760 Matrix Effects. Geostandards and Geoanalytical Research 40, 157–172.
761 https://doi.org/10.1111/j.1751-908X.2015.00364.x

762 Śliwiński, M.G., Kitajima, K., Kozdon, R., Spicuzza, M.J., Fournelle, J.H., Denny, A.C., Valley, J.W., 2016b.
763 Secondary Ion Mass Spectrometry Bias on Isotope Ratios in Dolomite–Ankerite, Part II: $\delta^{13}C$

764 Matrix Effects. Geostandards and Geoanalytical Research 40, 173–184.
765 https://doi.org/10.1111/j.1751-908X.2015.00380.x
766 Śliwiński, M.G., Kitajima, K., Spicuzza, M.J., Orland, I.J., Ishida, A., Fournelle, J.H., Valley, J.W., 2017b.
767 SIMS Bias on Isotope Ratios in Ca-Mg-Fe Carbonates (Part III): $\delta^{18}O$ and $\delta^{13}C$ Matrix Effects Along
768 the Magnesite–Siderite Solid-Solution Series. Geostandards and Geoanalytical Research 42, 49–
769 76. https://doi.org/10.1111/ggr.12194

770 Śliwiński, M.G., Schreiber, B.C., Ishida, A., Haroldson, E., Kuhn, P.P., Salazar-Jaramillo, S., Denny, A.C.,
771 Barnes, B.D., Spicuzza, M.J., Kitajima, K., Peters, S.E., Valley, J.W., 2019. Dolomitization of the
772 Middle Bakken Tight-oil Reservoir (Late Devonian – Early Mississippian, Williston Basin), 47.
773 http://www.geology.wisc.edu/homepages/wiscsims/public_html/pdfs/Sliwinski_Unpub2019.pd
774 f

775 Smith, M.G., Bustin, R.M., 2000. Late Devonian and Early Mississippian Bakken and Exshaw black shale
776 source rocks, Western Canada sedimentary basin: a sequence stratigraphic interpretation.
777 American Association of Petroleum Geologists Bulletin 84, 940–960.

778 Sonnenberg, S.A., 2011a. Chapter 11: TOC and Pyrolysis Data for the Bakken Shales, Williston Basin,
779 North Dakota and Montana, in: Robinson, J.W., LeFever, J.A., Gaswirth, S.B. (Eds.), The Bakken–
780 Three Forks Petroleum System in the Williston Basin. The Rocky Mountain Association of
781 Geologists, Denver, Colorado, pp. 308–331.

782 Sonnenberg, S.A., LeFever, J.A., Hill, R.J., 2011b. Chapter 15: Fracturing in the Bakken Petroleum System,
783 Williston Basin, in: Robinson, J.W., LeFever, J.A., Gaswirth, S.B. (Eds.), The Bakken–Three Forks
784 Petroleum System in the Williston Basin. The Rocky Mountain Association of Geologists, Denver,
785 Colorado, pp. 393–417.

786 Staruiala, A., Qing, H., Chi, G., Stern, R., Petts, D., 2013. Dolomite petrography and stable isotope
787 geochemistry of the Bakken Formation, southeastern Saskatchewan, in: Summary of
788 Investigations, Volume 1, Saskatchewan Geological Survey, Saskatchewan Ministry of the
789 Economy, Miscellaneous Report 2013-4.1, Paper A-8, 10 p.

790 Sun, S.Q., 1995. Dolomite Reservoirs: Porosity Evolution and Reservoir Characteristics. American
791 Association of Petroleum Geologists Bulletin 79, 186–204.

792 Surdam, R.C., Crossey, L.J., Hagen, E.S., Heasler, H.P., 1989. Organic-Inorganic Interactions and
793 Sandstone Diagenesis. American Association of Petroleum Geologists Bulletin 73, 1–23.

794 Swart, P.K., 2015. The geochemistry of carbonate diagenesis: The past, present and future.
795 Sedimentology 62, 1233–1304. https://doi.org/10.1111/sed.12205

796 Teboul, P.-A., Durlet, C., Girard, J.-P., Dubois, L., San Miguel, G., Virgone, A., Gaucher, E.C., Camoin, G.,
797 2019. Diversity and origin of quartz cements in continental carbonates: Example from the Lower
798 Cretaceous rift deposits of the South Atlantic margin. Applied Geochemistry 100, 22–41.
799 https://doi.org/10.1016/j.apgeochem.2018.10.019

800 Thyne, G.D., Boles, J.R., 1989. Isotopic evidence for origin of the Moeraki septarian concretions, New
801 Zealand. Journal of Sedimentary Research 59, 272–279. https://doi.org/10.1306/212F8F6C-
802 2B24-11D7-8648000102C1865D

803 Valley, J.W., Kita, N.T., 2009. In situ oxygen isotope geochemistry by ion microprobe. Mineralogical
804 Association of Canada Short Course 41, 19–63.

805 van Geldern, R., Joachimski, M.M., Day, J., Jansen, U., Alvarez, F., Yolkin, E.A., Ma, X.-P., 2006. Carbon,
806 oxygen and strontium isotope records of Devonian brachiopod shell calcite. Palaeogeography,
807 Palaeoclimatology, Palaeoecology, Evolution of the System Earth in the Late Palaeozoic: Clues
808 from Sedimentary Geochemistry 240, 47–67. https://doi.org/10.1016/j.palaeo.2006.03.045

Wang, X.-L., Coble, M.A., Valley, J.W., Shu, X.-J., Kitajima, K., Spicuzza, M.J., Sun, T., 2014. Influence of radiation damage on Late Jurassic zircon from southern China: Evidence from in situ measurements of oxygen isotopes, laser Raman, U–Pb ages, and trace elements. Chemical Geology 389, 122–136. https://doi.org/10.1016/j.chemgeo.2014.09.013

Warren, J., 2000. Dolomite: occurrence, evolution and economically important associations. Earth-Science Reviews 52, 1–81. https://doi.org/10.1016/S0012-8252(00)00022-2

Webster, R.L., 2011. Chapter 19: Petroleum Source Rocks and Stratigraphy of the Bakken Formation in North Dakota, in: Robinson, J.W., LeFever, J.A., Gaswirth, S.B. (Eds.), The Bakken–Three Forks Petroleum System in the Williston Basin. The Rocky Mountain Association of Geologists, Denver, Colorado, pp. 490–507.

Wentworth, C.K., 1922. A scale of grade and class terms for clastic sediments. The Journal of Geology 30, 377–392.

Williams, L.B., Hervig, R.L., Dutton, S.P., 1997. Constraints on Paleofluid Compositions in the Travis Peak Formation, East Texas: Evidence from Microanalyses of Oxygen Isotopes in Diagenetic Quartz, in: Basin-Wide Diagenetic Patterns: Integrated Petrologic, Geochemical, and Hydrologic Considerations, SEPM Special Publication. pp. 269–280.

Worden, R.H., Burley, S.D., 2003. Sandstone Diagenesis: The Evolution of Sand to Stone, in: Burley, S.D., Worden, R.H. (Eds.), Sandstone Diagenesis: Recent and Ancient. Blackwell Publishing Ltd., Oxford, UK, pp. 1–44.

FIGURES

Table 1. Name, depth, and location information for the 9 cores sampled.

Table 2. Ranges of isotopic data observed in each sample. A more detailed breakdown of isotopic trends in each sample may be found in the text.

Figure 1. Map of structure-depth contours for the Bakken Formation in western North Dakota, with the locations of drill core samples analyzed in this paper marked by stars. Note that contours displayed here are measured relative to sea level so as to best convey the basin's structure; all other depths reported in this paper are relative to the local surface elevation. The subsurface extent of the Bakken formation is marked with a dashed line. MT = Montana, ND = North Dakota. Figure modified from Sonnenberg et al., 2011a. See Table 1 for more information about sampling locations.

Figure 2. (a) Generalized stratigraphy of the Williston Basin, modified from Borcovsky et al. (2017). (b) Facies of the Bakken in studied drill cores, using the classification scheme of Egenhoff et al. (2011). Red dots denote the locations of samples selected for SIMS analysis. Color available in online version.

Figure 3. Histograms showing the distribution of all SIMS $\delta^{18}O$ analyses for each core. Plots are arranged from upper left to bottom right in the order from shallow to deep as described in the text. Bars are shaded by mineral.

Figure 4. Histograms showing the distribution of all SIMS $\delta^{13}C$ analyses for each core. Plots are arranged from upper left to bottom right in the order described in the text. Bars are shaded by mineral.

Figure 5. Crossplot for Bakken zoned ankerite-series cement SIMS data, showing paired $\delta^{18}O$ and $\delta^{13}C$ carbonate analyses that are shaded by (a) Fe#, and (b) growth zone. Only adjacent analyses were paired, making this dataset a subset of that presented in Figs. 4 and 5. The reference line shows the equilibrium dolomite compositions for variable temperature, if $\delta^{18}O_{water}$ = 0‰ and $\delta^{13}C_{CO2}$ = -7‰ (Horita, 2014). Color available in online version.

Figure 6. Crossplots, one for each core, showing the distributions of paired $\delta^{18}O$ and $\delta^{13}C$ analyses for both dolomite and calcite. Filled dots correspond to dolomite analyses and are shaded by Fe#; open grey dots correspond to calcite analyses. Only adjacent analyses were paired; this dataset is a subset of that presented in Figs. 4 and 5. Plots are arranged from upper left to bottom right in the order described in the text. Sample depths are indicated in each panel. Error bars are the 2SD precision measured on bracketing dolomite standard UW-6220. Color available in online version.

Figure 7. Histogram showing the distribution of SIMS $\delta^{18}O$ quartz analyses, classified using cathodoluminescence according to whether the analysis was made on detrital grains or quartz overgrowths.

Figure 8. Schematic ankerite-series crystal showing the three zones discussed in this paper. Darker grey indicates lower Fe/Mg. The Zone 1 to Zone 2 boundary can be either euhedral or rounded. See text for details.

Figure 9. Crossplots showing the distributions of paired $\delta^{18}O$ and $\delta^{13}C$ analyses (ankerite-series only) for each core, and colored by growth zone. Only adjacent analyses were paired, making this dataset a subset of that presented in Figs. 4 and 5. Plots are arranged from upper left to bottom right in the order described in the text. Sample depths are indicated in each panel. Arrows have been added to generalize changes in isotopic values from core out to the rim. Color available in online version.

Figure 10. Histogram showing the distribution of $\delta^{18}O$ and $\delta^{13}C$ values for Zone 1 dolomite cores classified according to the type of boundary they have with Zone 2.

Figure 11. SEM-BSE imagery overlain with SIMS analysis-pit locations for Well 1 (core 24883). SIMS pits are represented by ovals and are the size and shape of actual analysis pits; $\delta^{18}O$ pits are light pink and $\delta^{13}C$ pits are dark blue. Minerals are labeled as follows: Dol = Dolomite (endmember compositions), Ank = Ankerite-series carbonates, DQ = Detrital Quartz, Anh = Anhydrite. Boundaries between growth Zones 1, 2, and 3 are shown in representative locations. Detailed discussion of petrography for each sample is in the text. (a) Transect through an analyzed area of Well 1, with isotopic data (b) and Fe# (c) plotted. (d) Transect through an analyzed area of Well 1, with isotopic data (e) and Fe# (f) plotted.

Figure 12. SEM-BSE imagery overlain with SIMS analysis-pit locations for Well 2 (core 20249). SIMS pits are represented by ovals and are the size and shape of actual analysis pits; $\delta^{18}O$ pits are light pink and $\delta^{13}C$ pits are dark blue. Minerals are labeled as follows: Dol = Dolomite (endmember compositions), Ank = Ankerite-series carbonates, Cal = Calcite, Anh = Anhydrite. Boundaries between growth Zones 1, 2, and 3 are shown in representative locations. Detailed discussion of petrography for each sample is in the text, and more sample imagery may be found in Appendix C. (a) Transect through an analyzed area of Well 2, with isotopic data (b) and Fe# (c) plotted.

887 Figure 13. SEM-BSE imagery overlain with SIMS analysis-pit locations for Well 3 (core 17272). SIMS pits
888 are represented by ovals and are the size and shape of actual analysis pits; $\delta^{18}O$ pits are light pink and
889 $\delta^{13}C$ pits are dark blue. Minerals are labeled as follows: Dol = Dolomite (endmember compositions), Ank =
890 Ankerite-series carbonates, Cal = Calcite, OQ = Overgrowth (diagenetic) Quartz, DQ = Detrital Quartz.
891 Boundaries between growth Zones 1, 2, and 3 are shown in representative locations. Detailed discussion
892 of petrography for each sample is in the text, and more sample imagery may be found in Appendix C.
893 (a,b) Analyzed ankerite-series carbonates from Well 3. (c) Transect through an analyzed area of Well 3,
894 with isotopic data (d) and Fe# (e) plotted.

895 Figure 14. SEM-BSE imagery overlain with SIMS analysis-pit locations for Well 4 (core 17676). SIMS pits
896 are represented by ovals and are the size and shape of actual analysis pits; $\delta^{18}O$ pits are light pink and
897 $\delta^{13}C$ pits are dark blue. Minerals are labeled as follows: Dol = Dolomite (endmember compositions), Ank =
898 Ankerite-series carbonates, Cal = Calcite, OQ = Overgrowth (diagenetic) Quartz. Boundaries between
899 growth Zones 1, 2, and 3 are shown in representative locations. Detailed discussion of petrography for
900 each sample is in the text, and more sample imagery may be found in Appendix C. (a,b) Analyzed
901 ankerite-series carbonates from Well 4.

902

903 Figure 15a-i. (additional sample, petrography part 1 of 2, images a-i) Examples of sample SEM-BSE
904 imagery overlain with SIMS analysis-pit locations. SIMS pits are represented by ovals and are the size and
905 shape of actual analysis pits; $\delta^{18}O$ pits are light pink and $\delta^{13}C$ pits are dark blue. Minerals are labeled as
906 follows: Dol = Dolomite (endmember compositions), Ank = Ankerite-series carbonates, Cal = Calcite, DQ =
907 Detrital Quartz. Boundaries between growth Zones 1, 2, and 3 are shown in representative locations.
908 Detailed discussion of petrography for each sample is in the text, and more sample imagery may be found
909 in Appendix C. (a,b) Well 5 (core C16586), sampled at 2991 m. (c,d) Well 6 (core 17015), sampled at 3156
910 m. (e,f,g,h,i) Well 7 (core C21668), sampled at 3117 m (e,f) and 3119 m (g,h,i).

911

912 Figure 15j-p. (additional sample petrography, part 2 of 2, images j-p) Examples of sample SEM-BSE
913 imagery overlain with SIMS analysis-pit locations. SIMS pits are represented by ovals and are the size and
914 shape of actual analysis pits; $\delta^{18}O$ pits are light pink and $\delta^{13}C$ pits are dark blue. Minerals are labeled as
915 follows: Dol = Dolomite (endmember compositions), Ank = Ankerite-series carbonates, Cal = Calcite, DQ =
916 Detrital Quartz, OQ = Overgrowth (diagenetic) Quartz, Anh = Anhydrite, Py = Pyrite. Boundaries between

growth Zones 1, 2, and 3 are shown in representative locations. Detailed discussion of petrography for each sample is in the text, and more sample imagery may be found in Appendix C. (j,k,l) Well 8 (core 12785), sampled at 3449 m. Small round holes in (r) are locations where qualitative SEM-EDS measurements have damaged calcite. (u,v,w,x) Well 9 (core 22493), sampled at 3390 m (u,v) and 3401 m (w,x). Image (w) is a zoomed in region of (x).

Figure 16. Values of $\delta^{18}O$ for ankerite-series cements, colored by zone, and plotted by the maximum temperature each sample experienced as determined from burial models; plotted temperatures are not necessarily the temperatures that each cement stage grew at (Kuhn et al., 2012). Lines represent $\delta^{18}O$ water in equilibrium with dolomite at variable $\delta^{18}O$ and temperature (Horita, 2014); modern porewater possesses $\delta^{18}O$ values >5‰ (Peterman et al., 2017). Color available in online version. (a) Zone 1 dolomites show a similar spread of $\delta^{18}O$ values regardless of depth, indicating that they formed early in burial under similar temperature and fluid conditions. Assuming seawater fluid compositions at -1.5‰ yields a temperature range of Zone 1 formation of ~30 to 75°C. (b) Zone 2 dolomite $\delta^{18}O$ values develop a slant that shows similarity to curves for high-$\delta^{18}O$ water, presumably as burial and water-rock interaction advance. (c) Zone 3 dolomite continues the Zone 2 trend at depth, but Well 1 shows a sequence of chemical zonation indicative of fluid passage (see text for discussion).

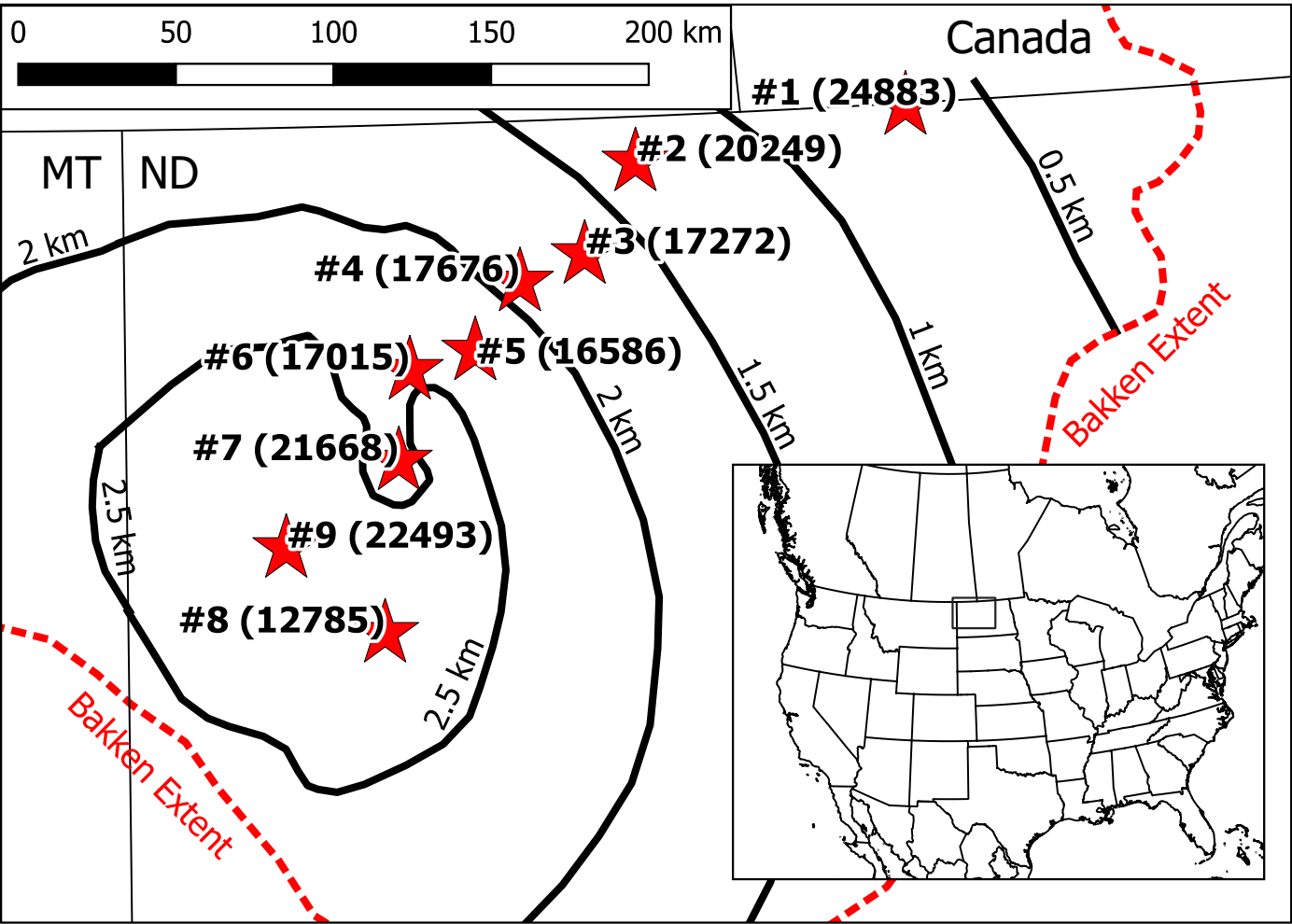
0
50
100
150
200 km
Canada
MT
ND
#1 (24883)
#2 (20249)
#3 (17272)
#4 (17676)
#5 (16586)
#6 (17015)
#7 (21668)
#9 (22493)
#8 (12785)
0.5 km
1 km
1.5 km
2 km
2.5 km
2 km
2.5 km
Bakken Extent
Bakken Extent

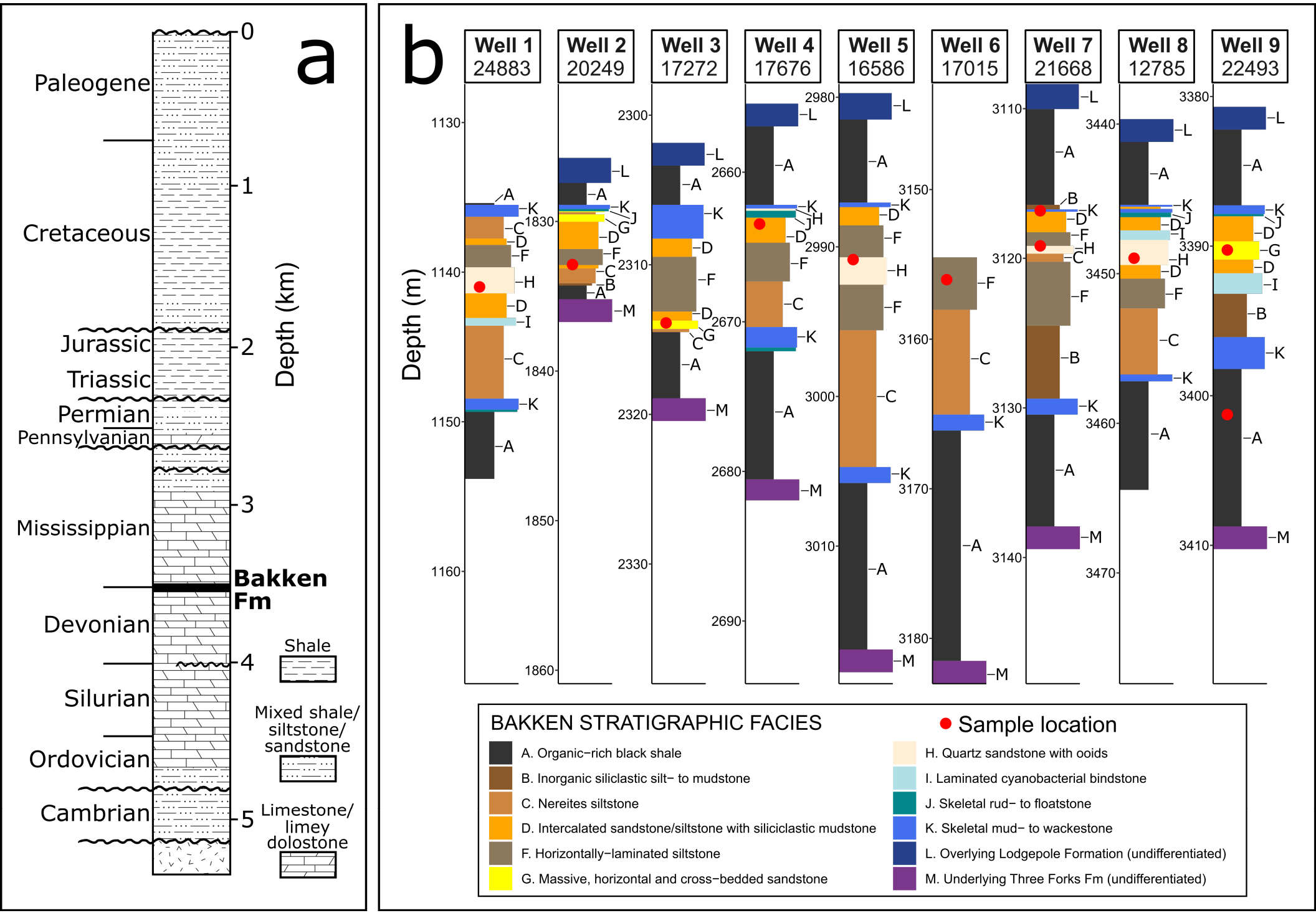
a
Paleogene
Cretaceous
Jurassic
Triassic
Permian
Pennsylvanian
Mississippian
Bakken Fm
Devonian
Silurian
Ordovician
Cambrian
0
1
2
3
4
5
Depth (km)
Shale
Mixed shale/ siltstone/ sandstone
Limestone/ limey dolostone
b
Well 1 24883
Well 2 20249
Well 3 17272
Well 4 17676
Well 5 16586
Well 6 17015
Well 7 21668
Well 8 12785
Well 9 22493
Depth (m)
BAKKEN STRATIGRAPHIC FACIES
A. Organic−rich black shale
B. Inorganic siliclastic silt− to mudstone
C. Nereites siltstone
D. Intercalated sandstone/siltstone with siliciclastic mudstone
F. Horizontally−laminated siltstone
G. Massive, horizontal and cross−bedded sandstone
H. Quartz sandstone with ooids
I. Laminated cyanobacterial bindstone
J. Skeletal rud− to floatstone
K. Skeletal mud− to wackestone
L. Overlying Lodgepole Formation (undifferentiated)
M. Underlying Three Forks Fm (undifferentiated)
Sample location

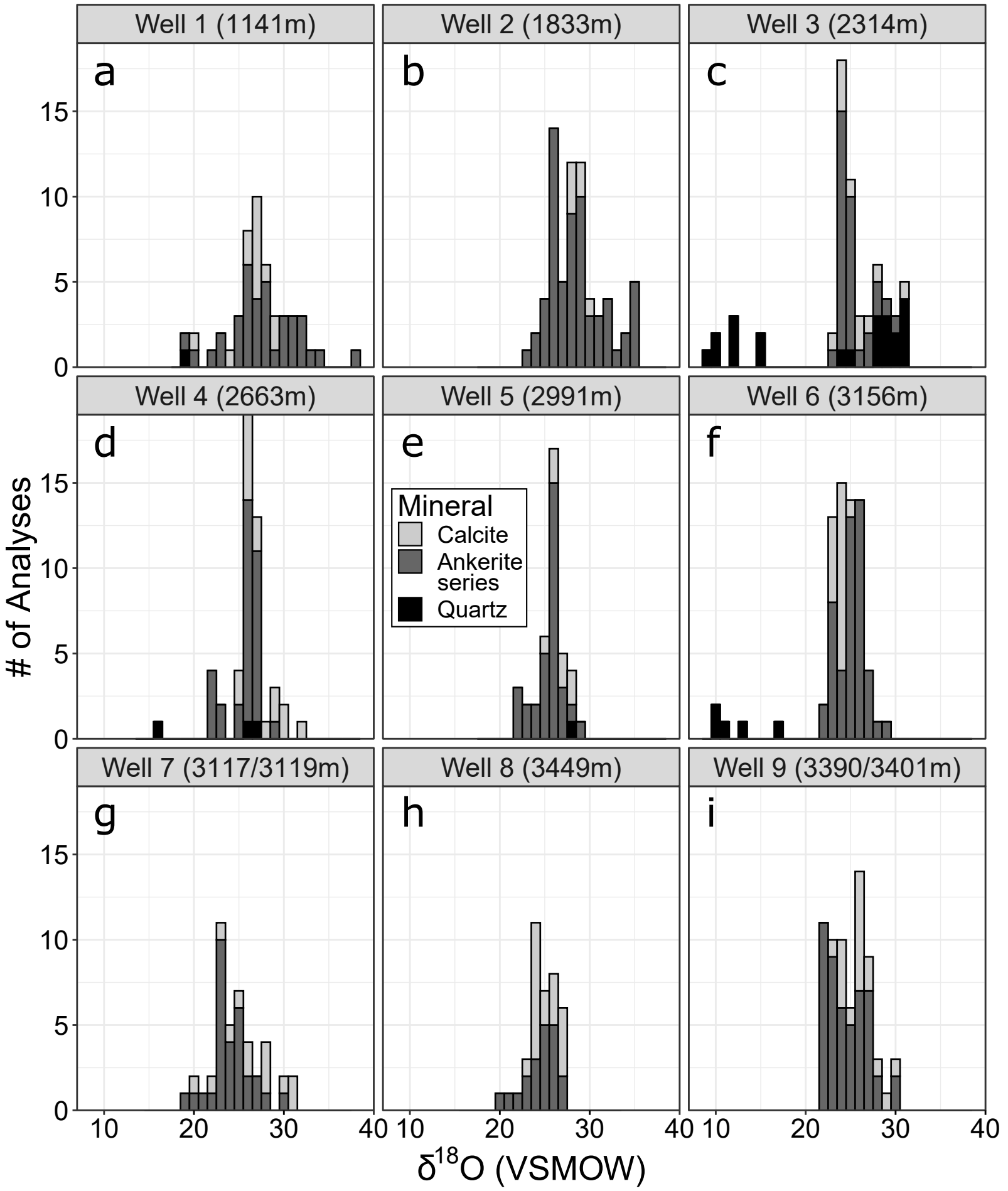
Well 1 (1141m)
Well 2 (1833m)
Well 3 (2314m)
Well 4 (2663m)
Well 5 (2991m)
Well 6 (3156m)
Well 7 (3117/3119m)
Well 8 (3449m)
Well 9 (3390/3401m)
a
b
c
d
e
f
g
h
i
Mineral
Calcite
Ankerite series
Quartz
# of Analyses
0
5
10
15
10
20
30
40
δ18O (VSMOW)

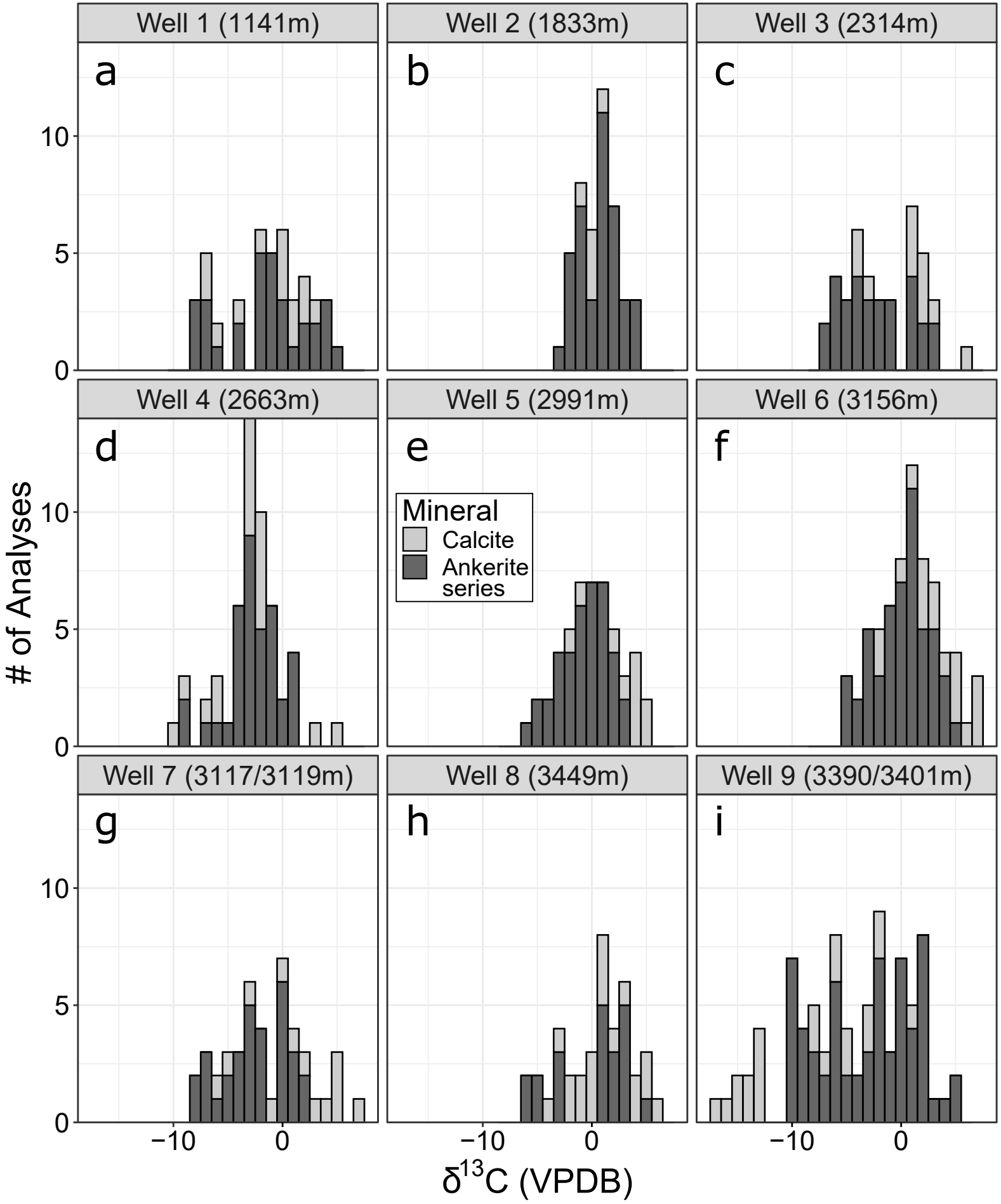
Well 1 (1141m)
Well 2 (1833m)
Well 3 (2314m)
Well 4 (2663m)
Well 5 (2991m)
Well 6 (3156m)
Well 7 (3117/3119m)
Well 8 (3449m)
Well 9 (3390/3401m)
a
b
c
d
e
f
g
h
i
Mineral
Calcite
Ankerite series
# of Analyses
0
5
10
−10
0
δ13C (VPDB)

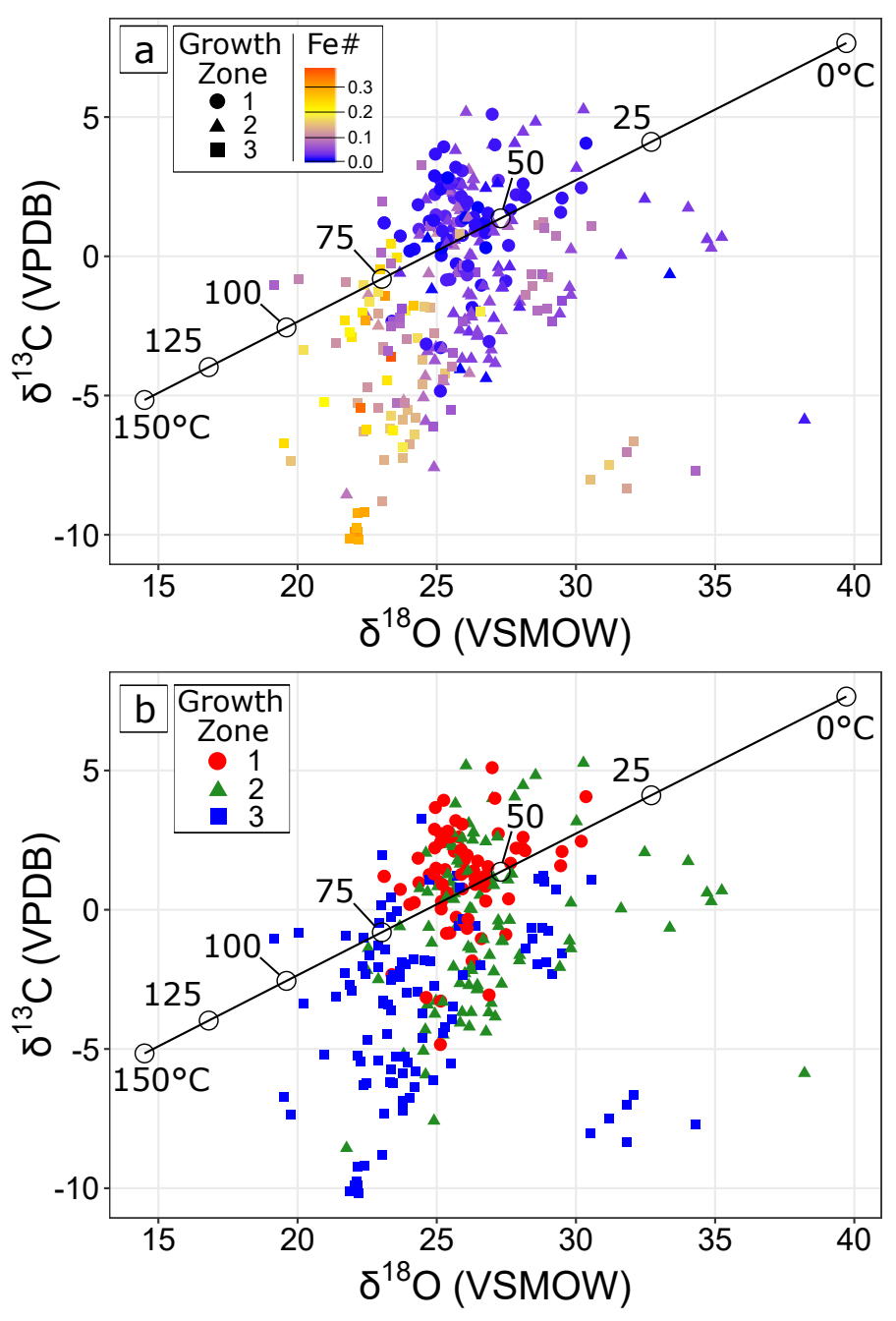
a
Growth Zone
1
2
3
Fe#
0.3
0.2
0.1
0.0
0°C
25
50
75
100
125
150°C
δ13C (VPDB)
δ18O (VSMOW)
5
0
-5
-10
15
20
25
30
35
40
b
Growth Zone
1
2
3
0°C
25
50
75
100
125
150°C
δ13C (VPDB)
δ18O (VSMOW)

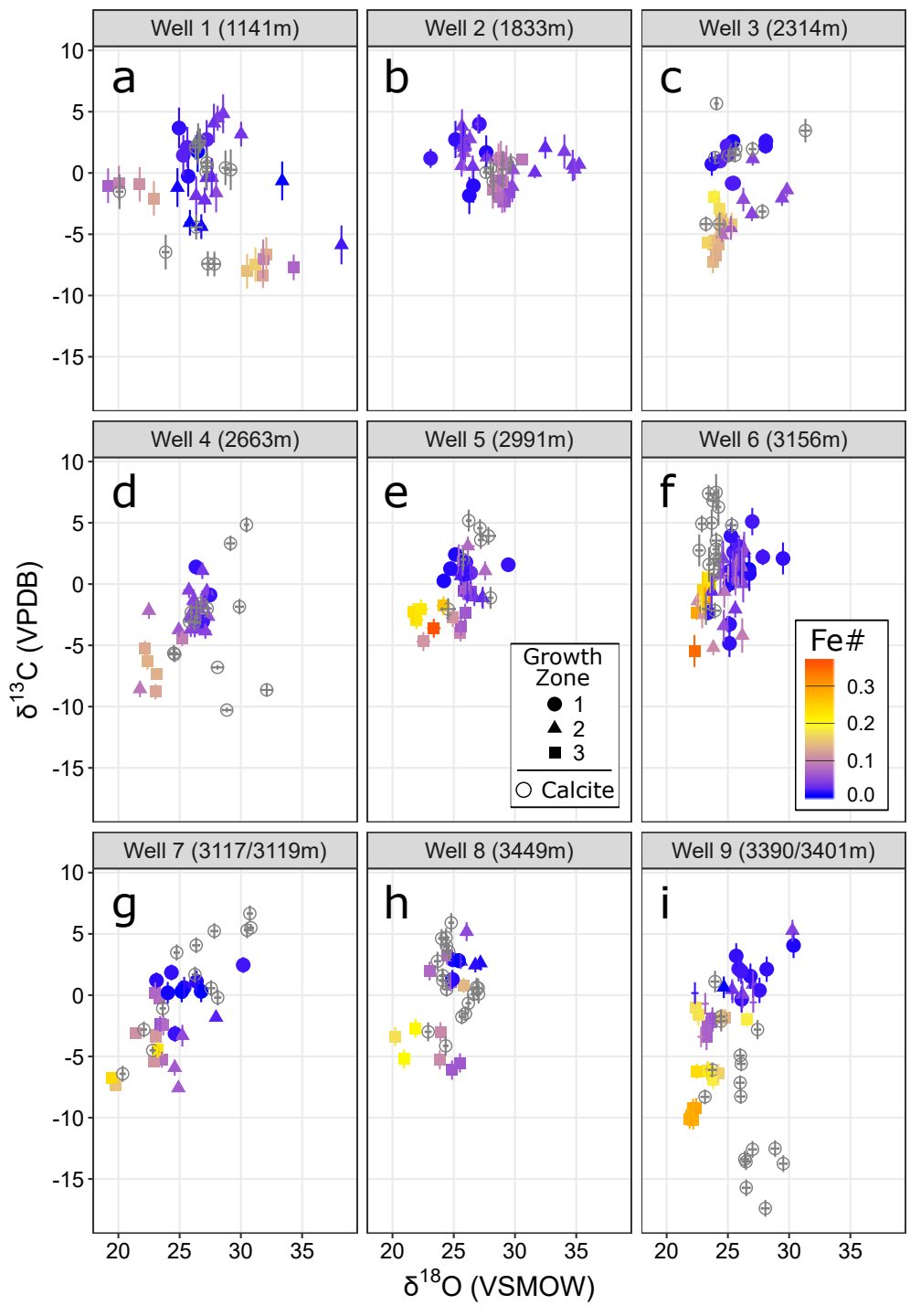
Well 1 (1141m)
Well 2 (1833m)
Well 3 (2314m)
Well 4 (2663m)
Well 5 (2991m)
Well 6 (3156m)
Well 7 (3117/3119m)
Well 8 (3449m)
Well 9 (3390/3401m)
a
b
c
d
e
f
g
h
i
Growth Zone
1
2
3
Calcite
Fe#
0.3
0.2
0.1
0.0
δ13C (VPDB)
δ18O (VSMOW)
10
5
0
-5
-10
-15
20
25
30
35

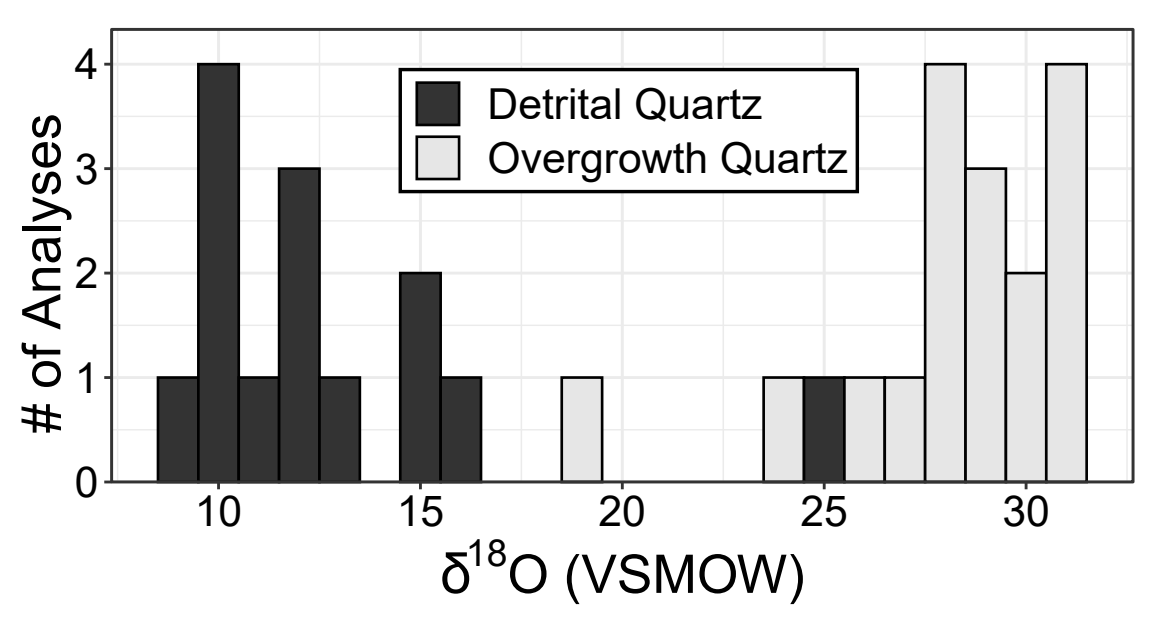
Detrital Quartz
Overgrowth Quartz
# of Analyses
0
1
2
3
4
10
15
20
25
30
δ18O (VSMOW)

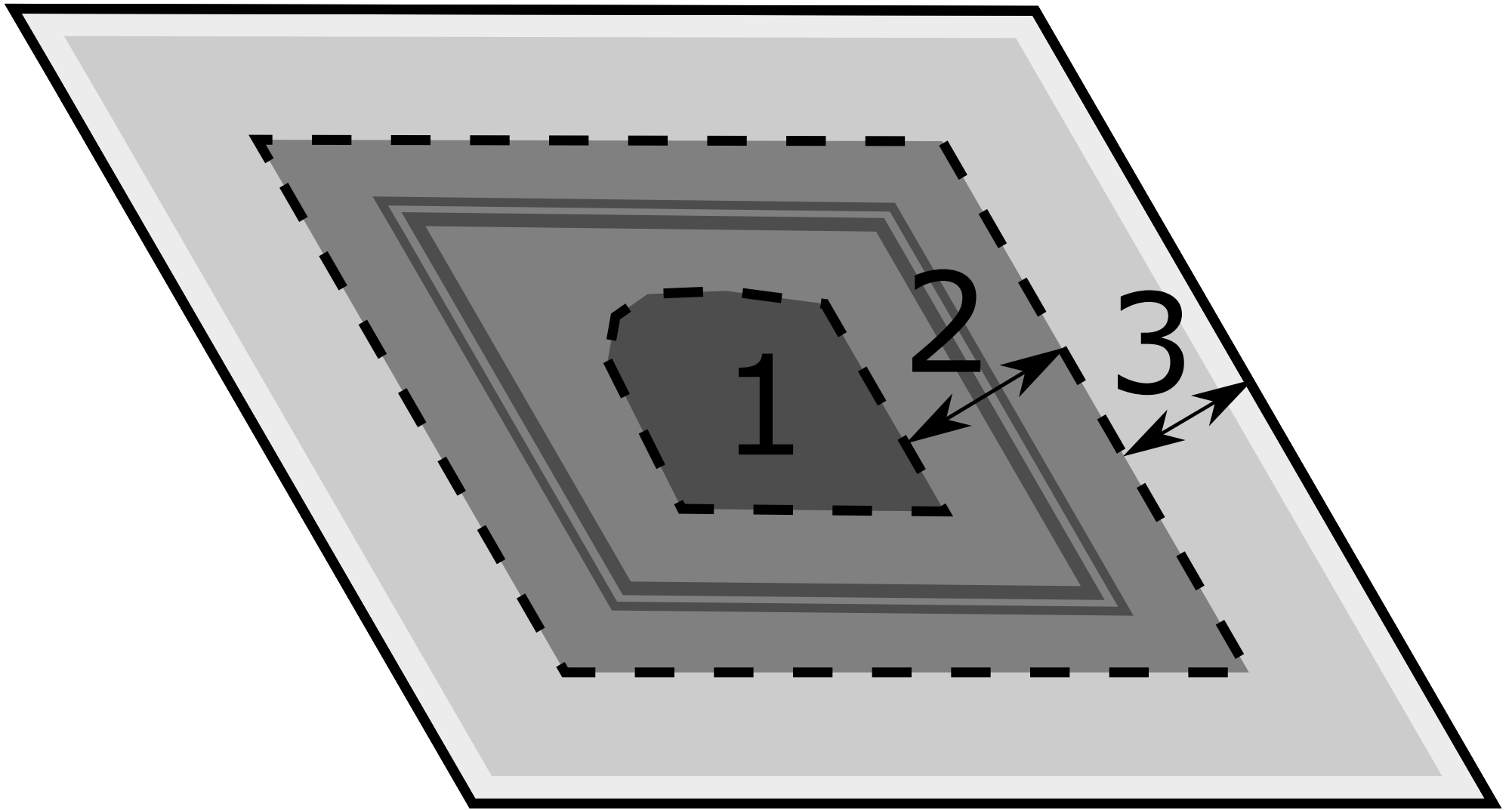
1
2
3

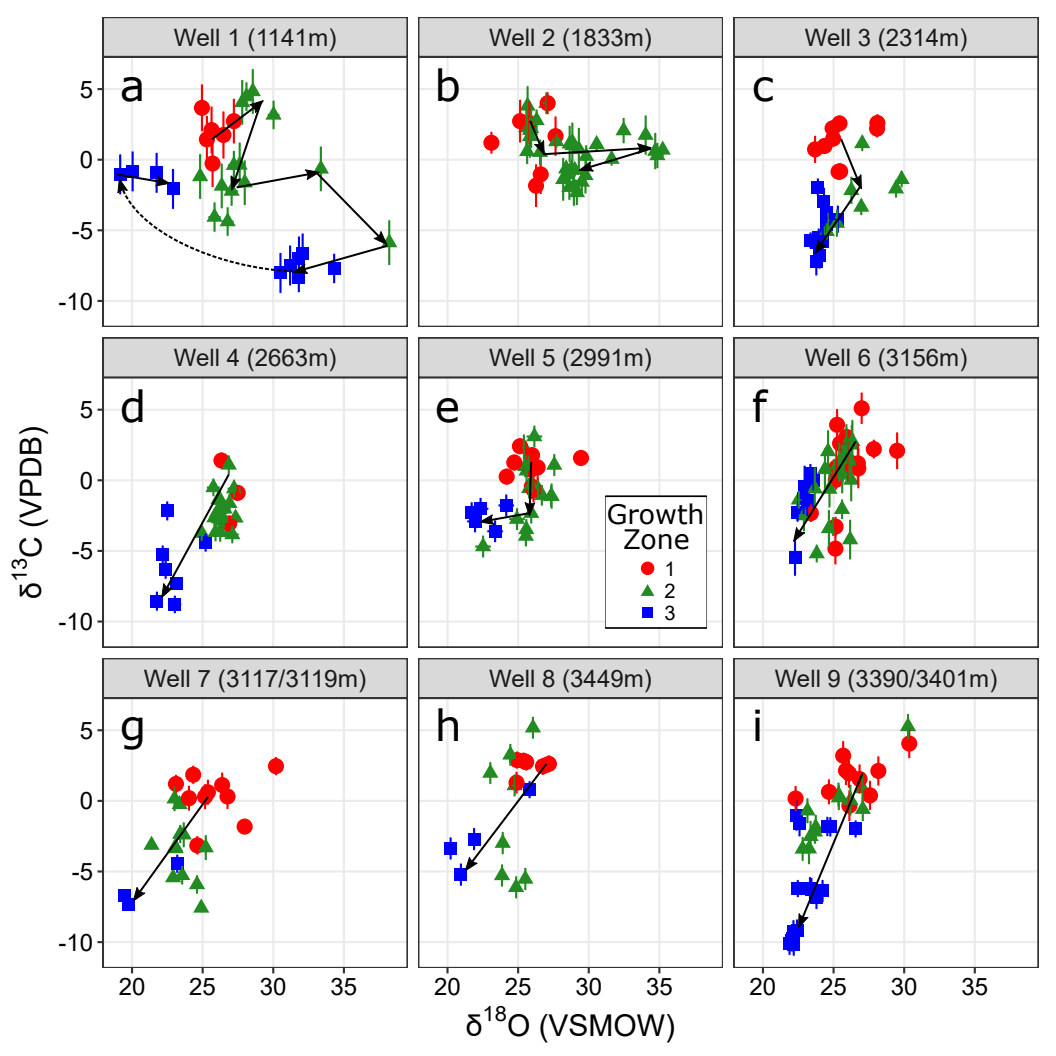
Well 1 (1141m)
Well 2 (1833m)
Well 3 (2314m)
Well 4 (2663m)
Well 5 (2991m)
Well 6 (3156m)
Well 7 (3117/3119m)
Well 8 (3449m)
Well 9 (3390/3401m)
a
b
c
d
e
f
g
h
i
Growth Zone
1
2
3
δ13C (VPDB)
δ18O (VSMOW)
5
0
-5
-10
20
25
30
35

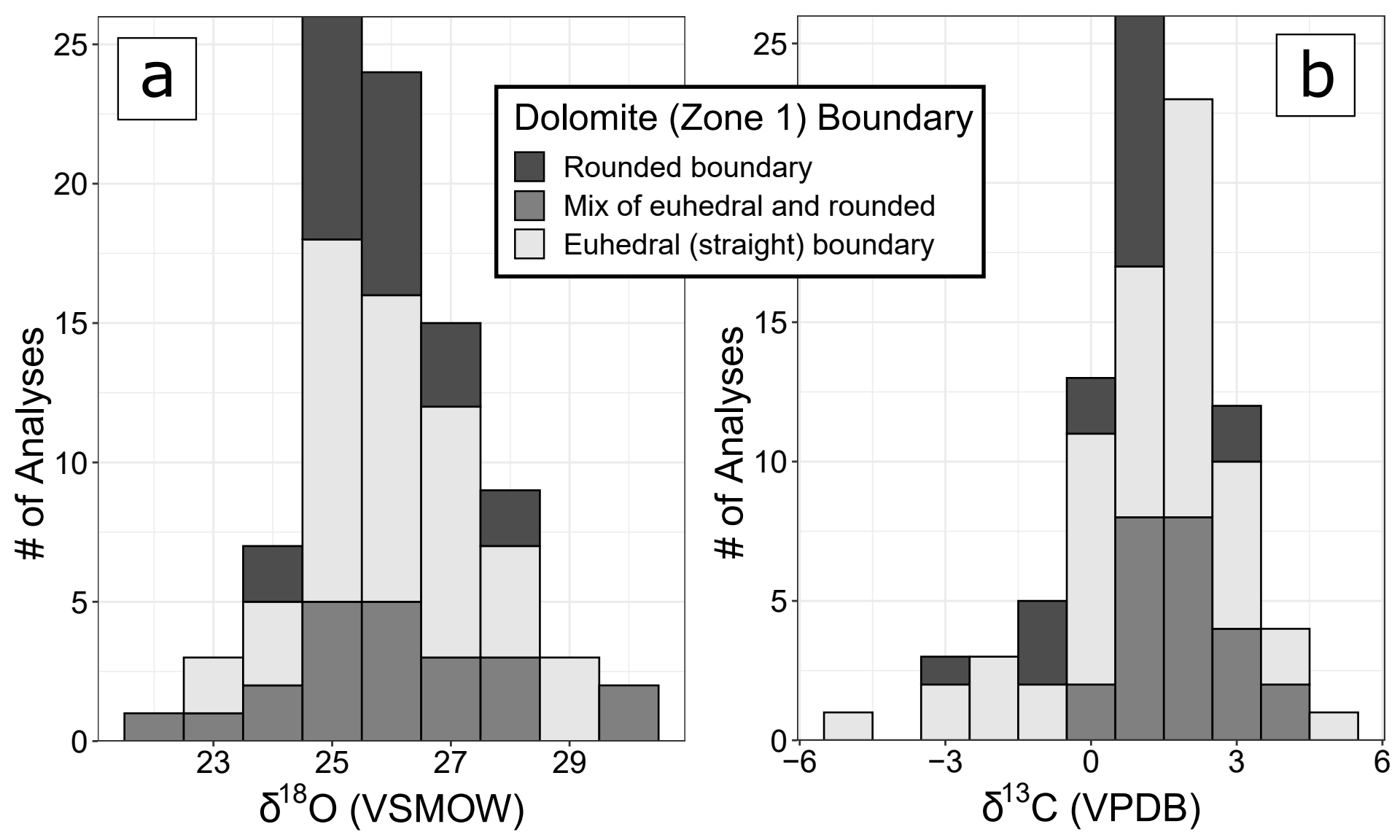
a
b
Dolomite (Zone 1) Boundary
Rounded boundary
Mix of euhedral and rounded
Euhedral (straight) boundary
# of Analyses
δ18O (VSMOW)
δ13C (VPDB)
0
5
10
15
20
25
23
25
27
29
−6
−3
0
3
6

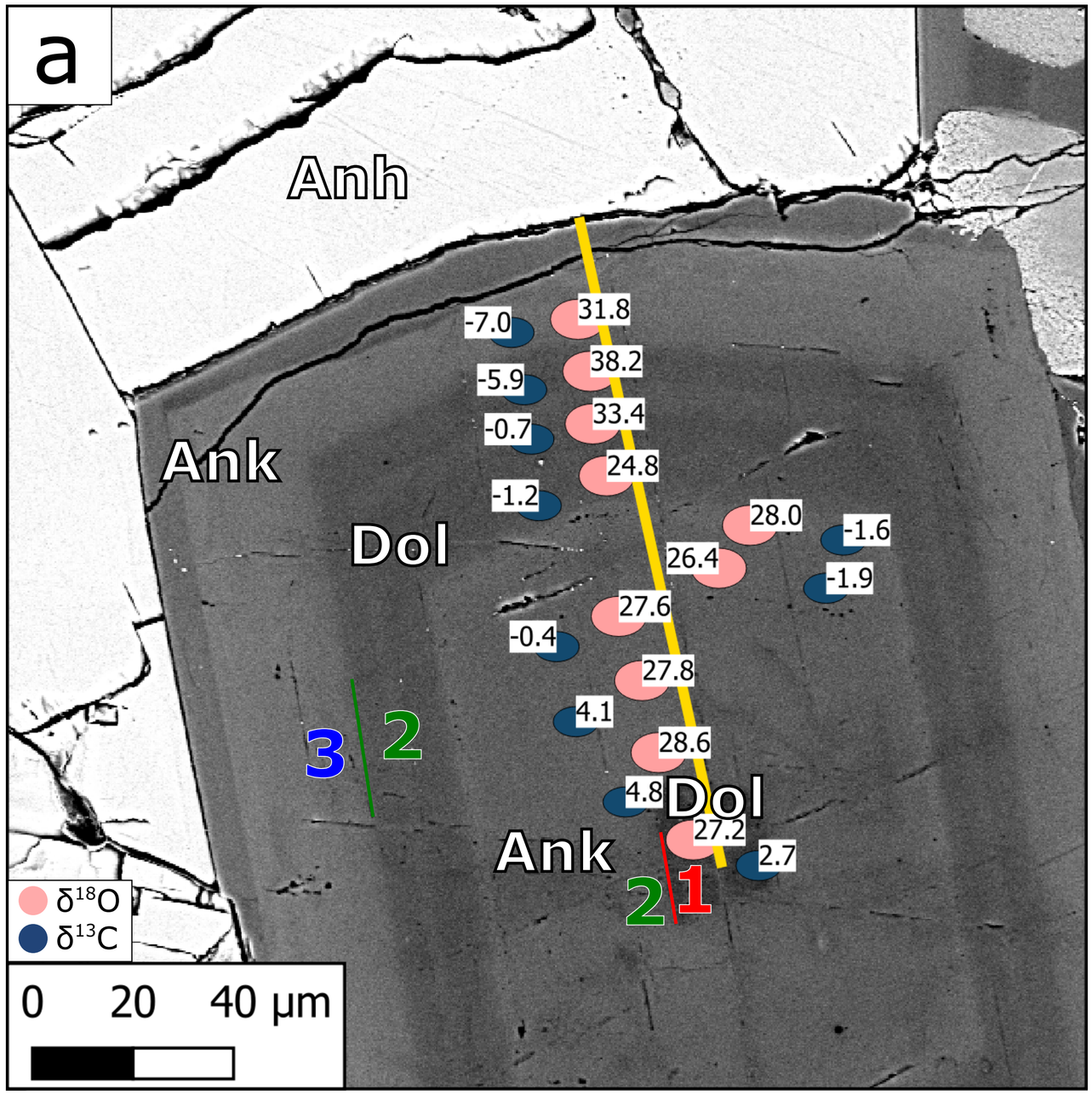
a
Anh
Ank
Dol
Dol
Ank
3
2
2
1
-7.0
31.8
-5.9
38.2
-0.7
33.4
-1.2
24.8
28.0
-1.6
26.4
-1.9
27.6
-0.4
27.8
4.1
28.6
4.8
27.2
2.7
δ18O
δ13C
0 20 40 μm

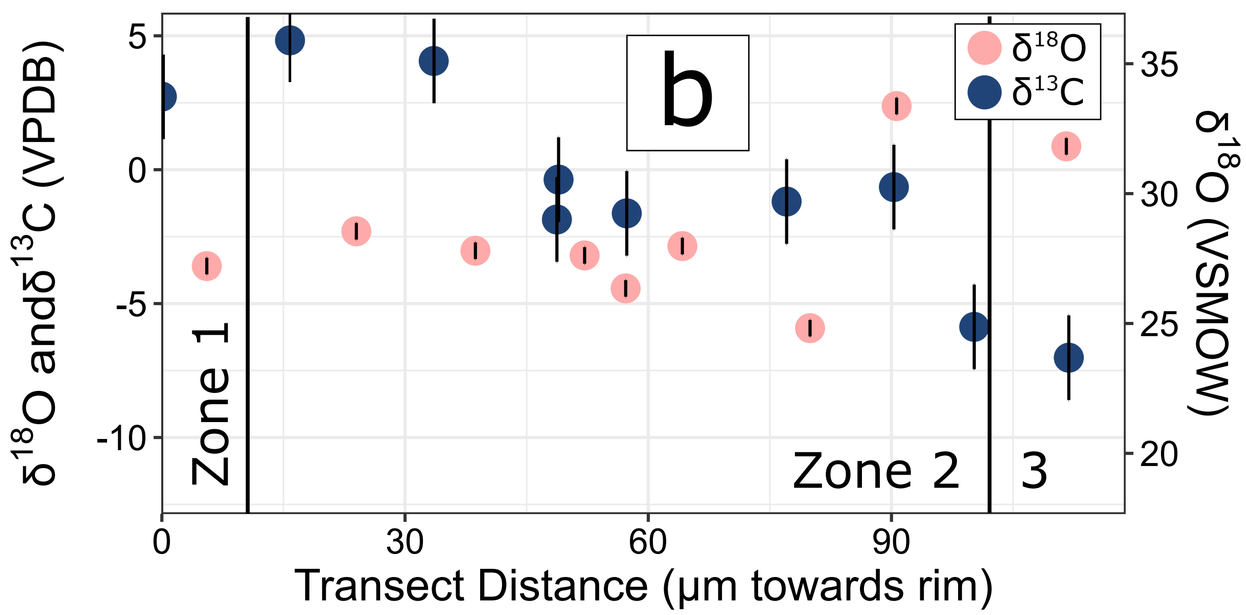
b
δ18O
δ13C
Zone 1
Zone 2
3
δ18O and δ13C (VPDB)
δ18O (VSMOW)
Transect Distance (μm towards rim)

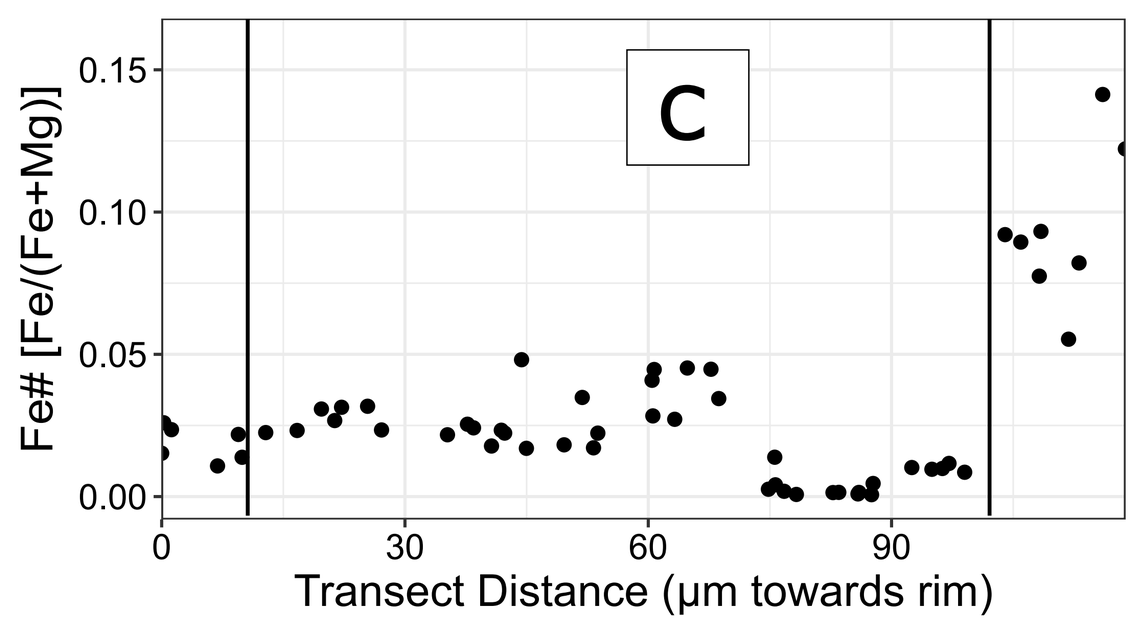
c
Fe# [Fe/(Fe+Mg)]
Transect Distance (μm towards rim)

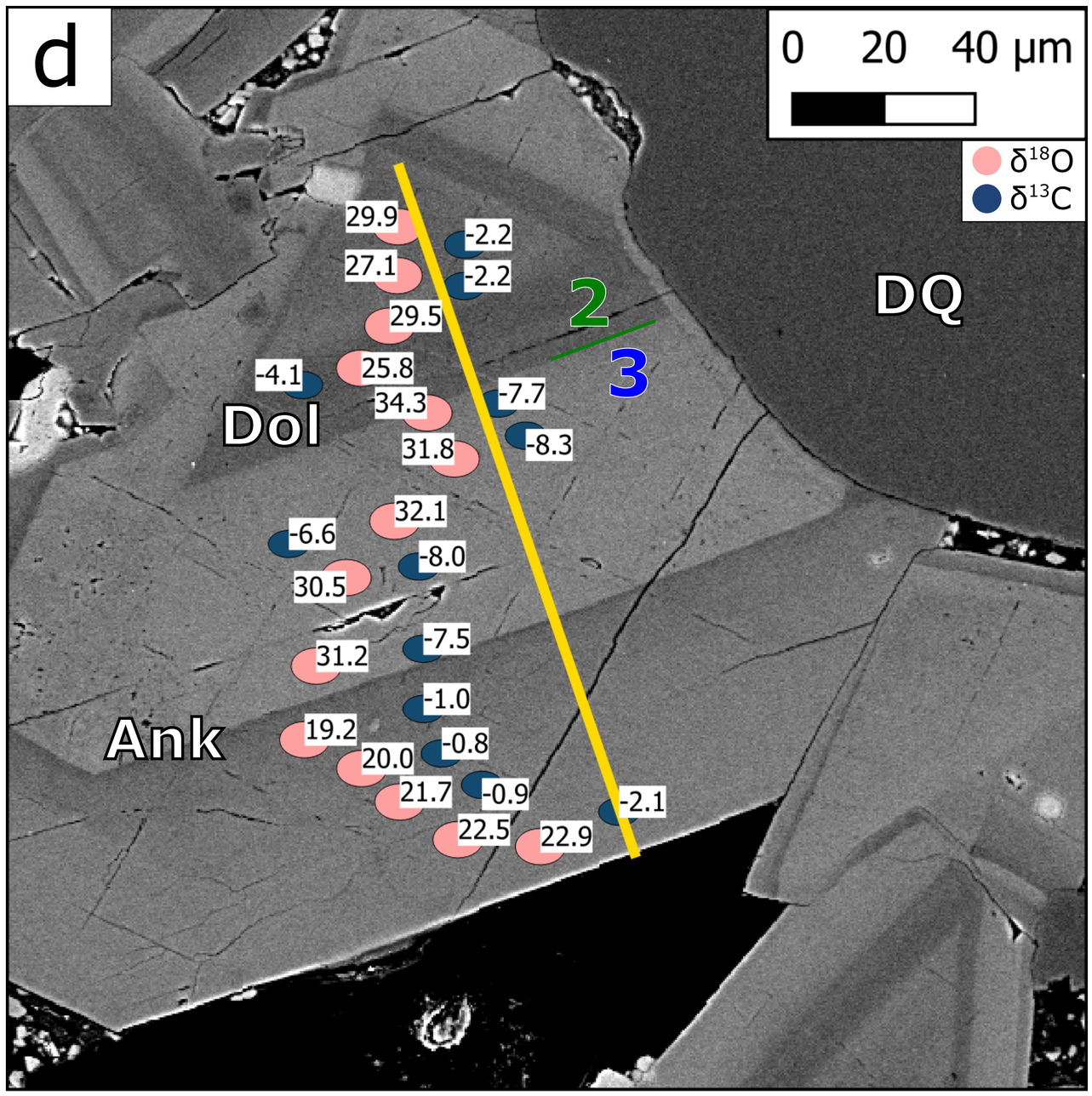
d
0 20 40 μm
δ18O
δ13C
DQ
Dol
Ank
2
3
29.9
-2.2
27.1
-2.2
29.5
25.8
-4.1
34.3
-7.7
31.8
-8.3
32.1
-6.6
-8.0
30.5
-7.5
31.2
-1.0
19.2
-0.8
20.0
21.7
-0.9
22.5
22.9
-2.1

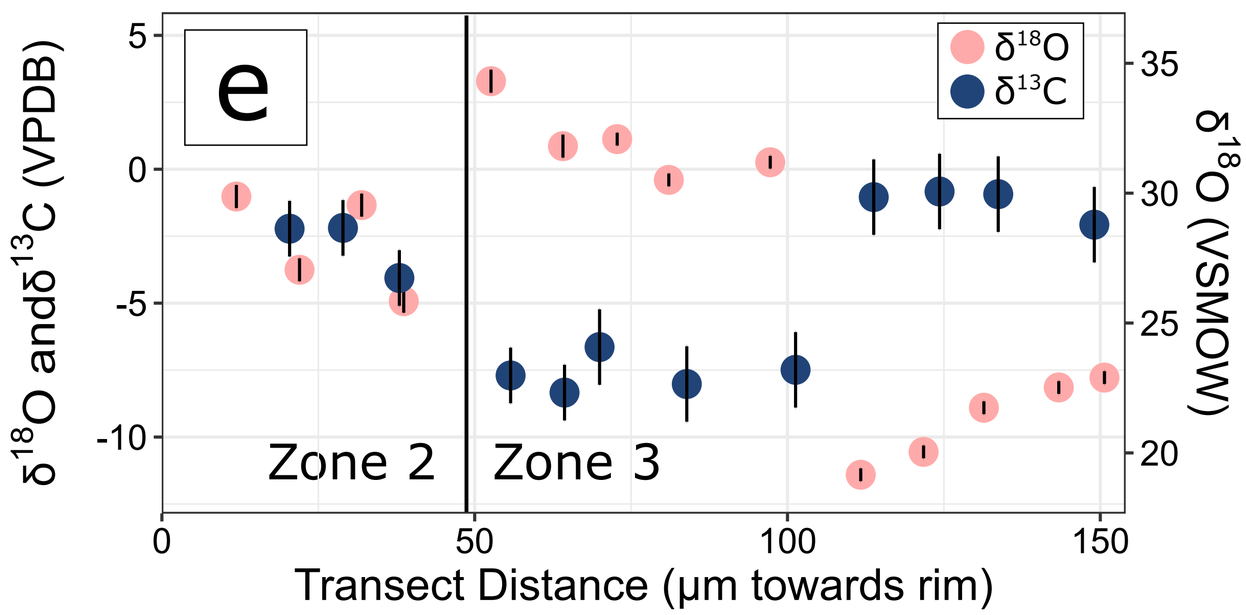
e
δ18O
δ13C
Zone 2
Zone 3
δ18O and δ13C (VPDB)
δ18O (VSMOW)
Transect Distance (μm towards rim)

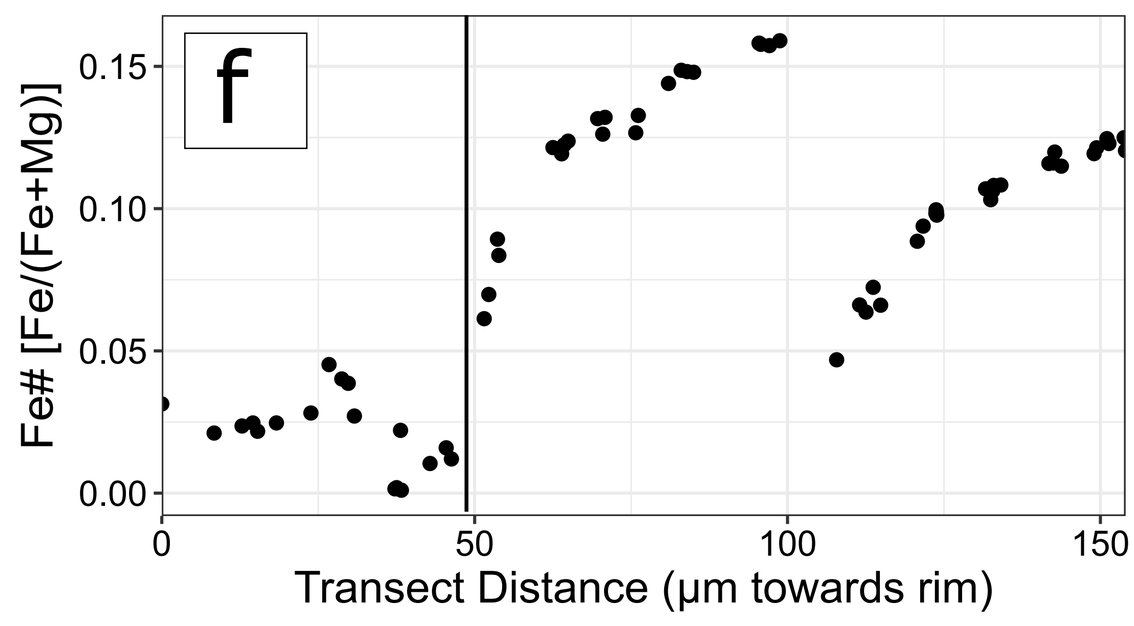
f
Fe# [Fe/(Fe+Mg)]
Transect Distance (μm towards rim)

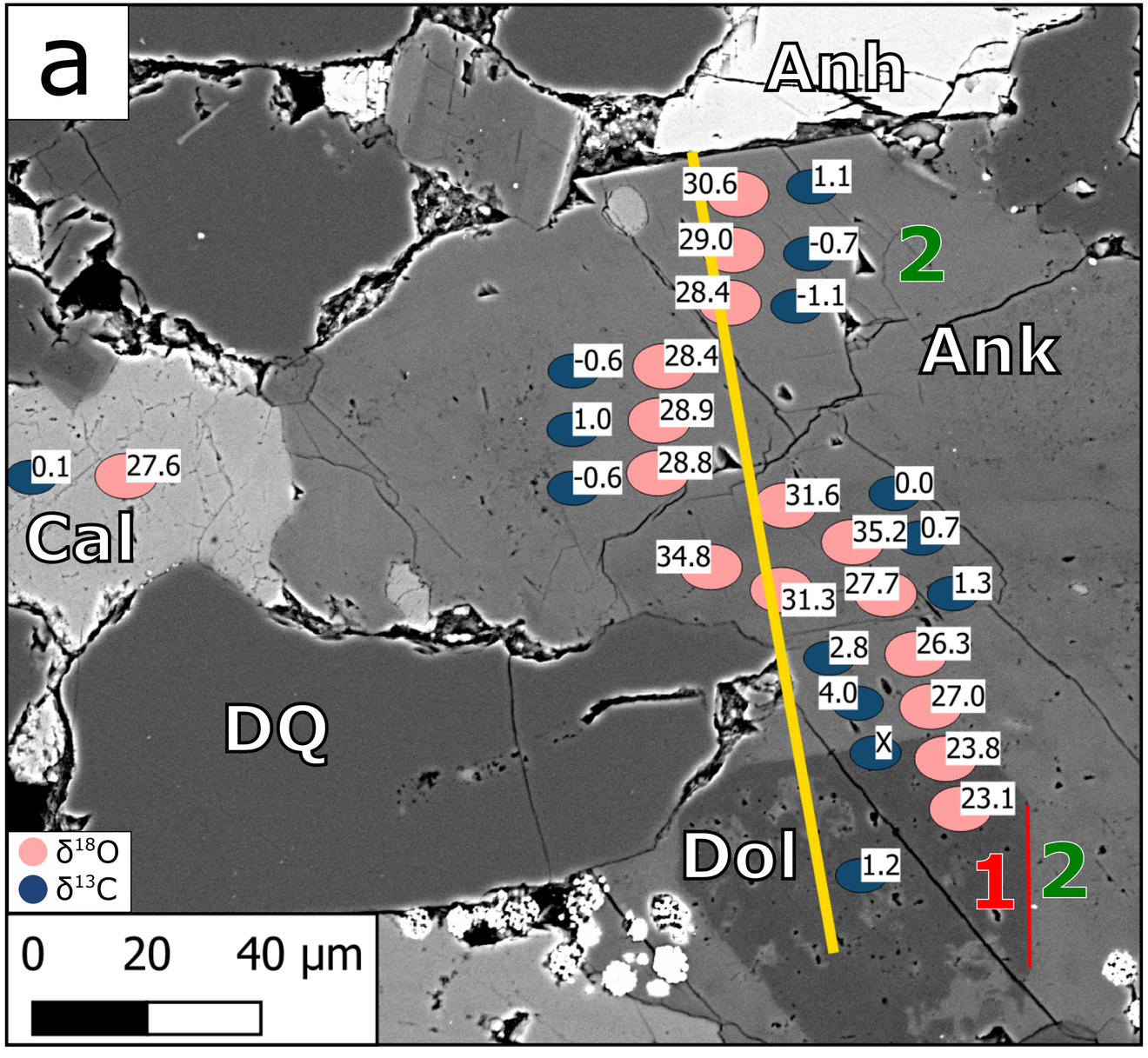
a
Anh
Ank
Cal
DQ
Dol
30.6
1.1
29.0
-0.7
28.4
-1.1
-0.6
28.4
1.0
28.9
-0.6
28.8
0.1
27.6
31.6
0.0
35.2
0.7
34.8
31.3
27.7
1.3
2.8
26.3
4.0
27.0
X
23.8
23.1
1.2
1
2
2
δ18O
δ13C
0 20 40 µm

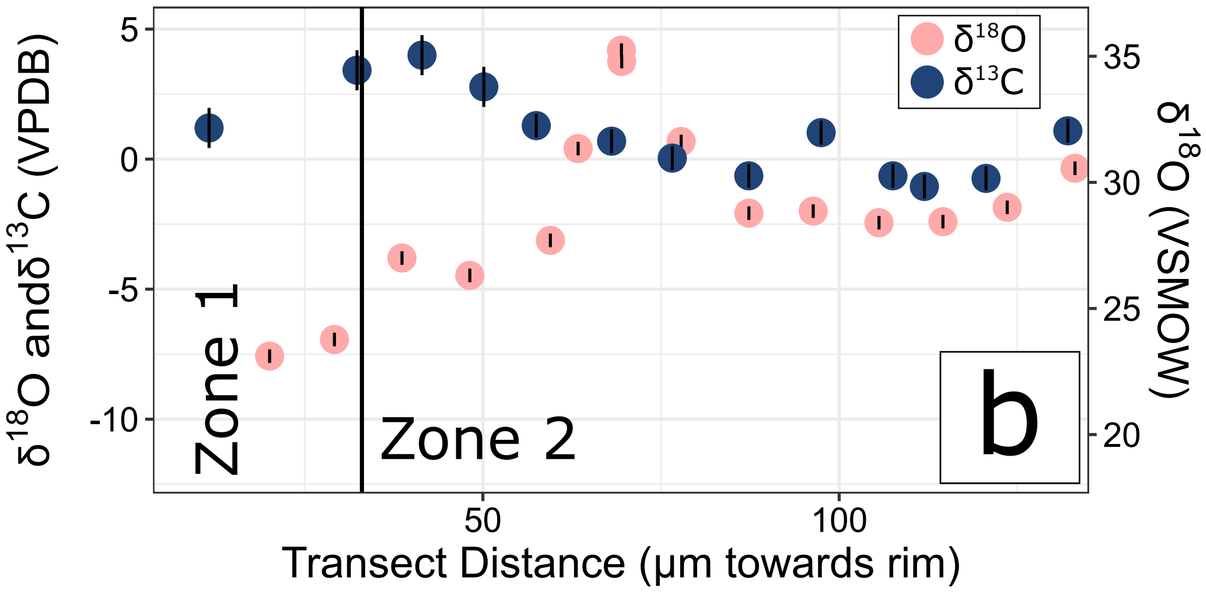
δ18O
δ13C
Zone 1
Zone 2
b
δ18O andδ13C (VPDB)
δ18O (VSMOW)
Transect Distance (µm towards rim)

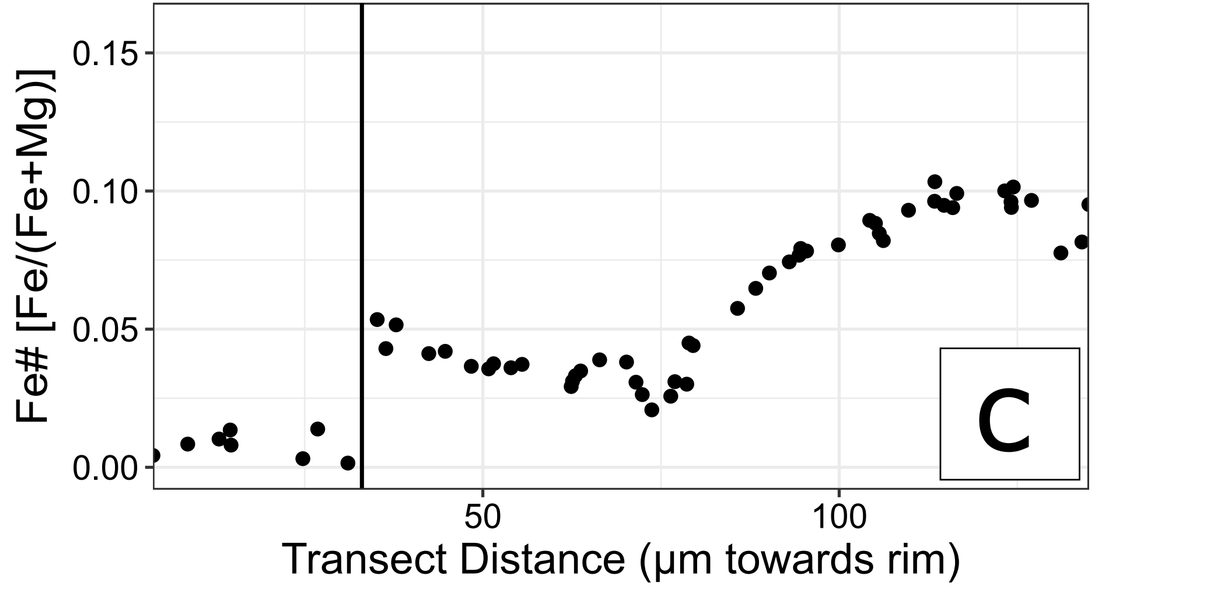
c
Fe# [Fe/(Fe+Mg)]
Transect Distance (µm towards rim)

a

δ18O
δ13C

Cal
Ank
Dol
DQ
OQ
1
2
1.9
27.0
-1.9
23.9
-5.5
-5.9
23.9
23.8
-4.9
23.7
X
24.2
2.2
28.1
-2.1
29.4
28.1
2.6
2.0
25.6
23.2
-4.2
9.2
28.9
0 20 40 µm

b

δ18O
δ13C

DQ
OQ
DQ
Ank
DQ
Dol
Cal
1
2
3
9.5
31.5
-3.7
-4.6
-4.3
1.1
24.5
24.5
24.6
27.0
24.4
25.0
-2.8
1.0
1.5
24.1
5.7
11.7
0 20 40 µm

c

δ18O
δ13C

Dol
DQ
Ank
Cal
1
2
2
3
-0.8
25.4
-0.8
25.5
29.8
25.2
23.8
25.3
-1.4
-4.5
-7.2
-4.2
31.3
3.5
0 20 40 µm

d

δ18O
δ13C

δ18O and δ13C (VPDB)
δ18O (VSMOW)
5
0
-5
-10
35
30
25
20
Zone 1
Zone 2
Zone 3
25
50
75
Transect Distance (µm towards rim)

e

Fe# [Fe/(Fe+Mg)]
0.15
0.10
0.05
0.00
25
50
75
Transect Distance (µm towards rim)

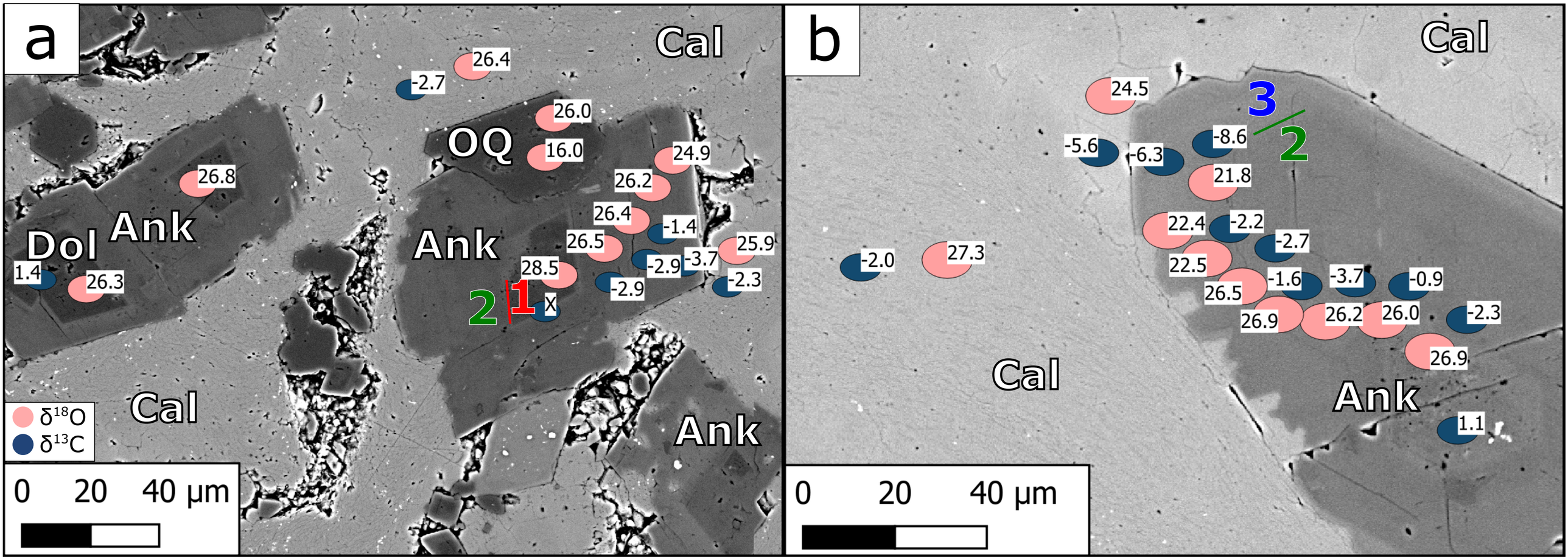
a
Cal
OQ
Ank
Dol
Ank
Cal
Ank
26.4
-2.7
26.0
16.0
24.9
26.8
26.2
26.4
-1.4
26.5
25.9
-3.7
28.5
-2.9
-2.3
-2.9
1.4
26.3
2
1
X
δ18O
δ13C
0 20 40 µm
b
Cal
24.5
3
2
-8.6
-5.6
-6.3
21.8
22.4
-2.2
-2.7
-2.0
27.3
22.5
-1.6
-3.7
-0.9
26.5
26.9
26.2
26.0
-2.3
26.9
Cal
Ank
1.1
0 20 40 µm

a
DQ
Cal
Ank
Cal
5.2
26.2
25.6
25.5
0.7
1.0
-1.1
28.0
3.1
26.1
2.4
25.4
-0.0
3.3
27.6
1.1
-1.1
27.3
-1.1
26.7
26.4
-0.6
26.0
-0.6
-0.3
25.8
-2.3
25.9
-3.5
25.6
-4.0
25.6
21.7
-2.3
27.8
3.9
-2.0
22.3
24.9
-5.4
22.5
-2.8
-5.9
-4.7
24.5
24.2
21.9
-2.9
-3.6
2
3
0 20 40 µm

b
Cal
Ank
DQ
Cal
3.3
-2.7
25.9
-0.3
25.7
1.2
0.1
26.1
27.4
-1.1
0.1
-0.7
26.4
0.9
4.5
26.0
-0.4
1
2
Dol
δ18O
δ13C
0 20 40 µm

c
Cal
Dol
DQ
26.2
0.0
2.8
26.3
DQ
-0.6
2
1
23.7
24.6
Ank
1.4
2.0
24.4
26.1
24.7
0.8
25.6
-0.6
24.7
0.4
-3.4
Cal
23.9
0.8
23.2
-2.0
0 20 40 µm

d
Dol
DQ
-2.0
25.6
Ank
1.8
25.7
-0.2
X
25.7
0.8
X
23.4
2
1
2
23.6
0.5
3
-0.0
23.4
7.4
Cal
23.8
6.8
DQ
0 20 40 µm

e
Cal
Ank
-5.3
23.6
Ank
-5.9
2
24.6
-6.9
-4.0
3
-3.1
2
24.6
1
Dol
0 20 40 µm

f
-6.4
20.4
Cal
-6.7
19.5
22.1
3
-8.2
X
Ank
2
-2.8
-7.4
19.8
-3.1
21.4
23.6
-3.4
23.1
-1.1
Cal
-3.3
23.1
Ank
0 20 40 µm

g
DQ
24.3
1
1.9
1.2
23.1
2
-2.4
23.4
3
23.2
-4.5
Cal
0 20 40 µm

h
Cal
0.6
27.6
5.2
27.8
Cal
26.4
4.1
0 10 µm

i
Ank
0 10 µm
23.4
0.5
-2.1
Ank
22.8
DQ
X

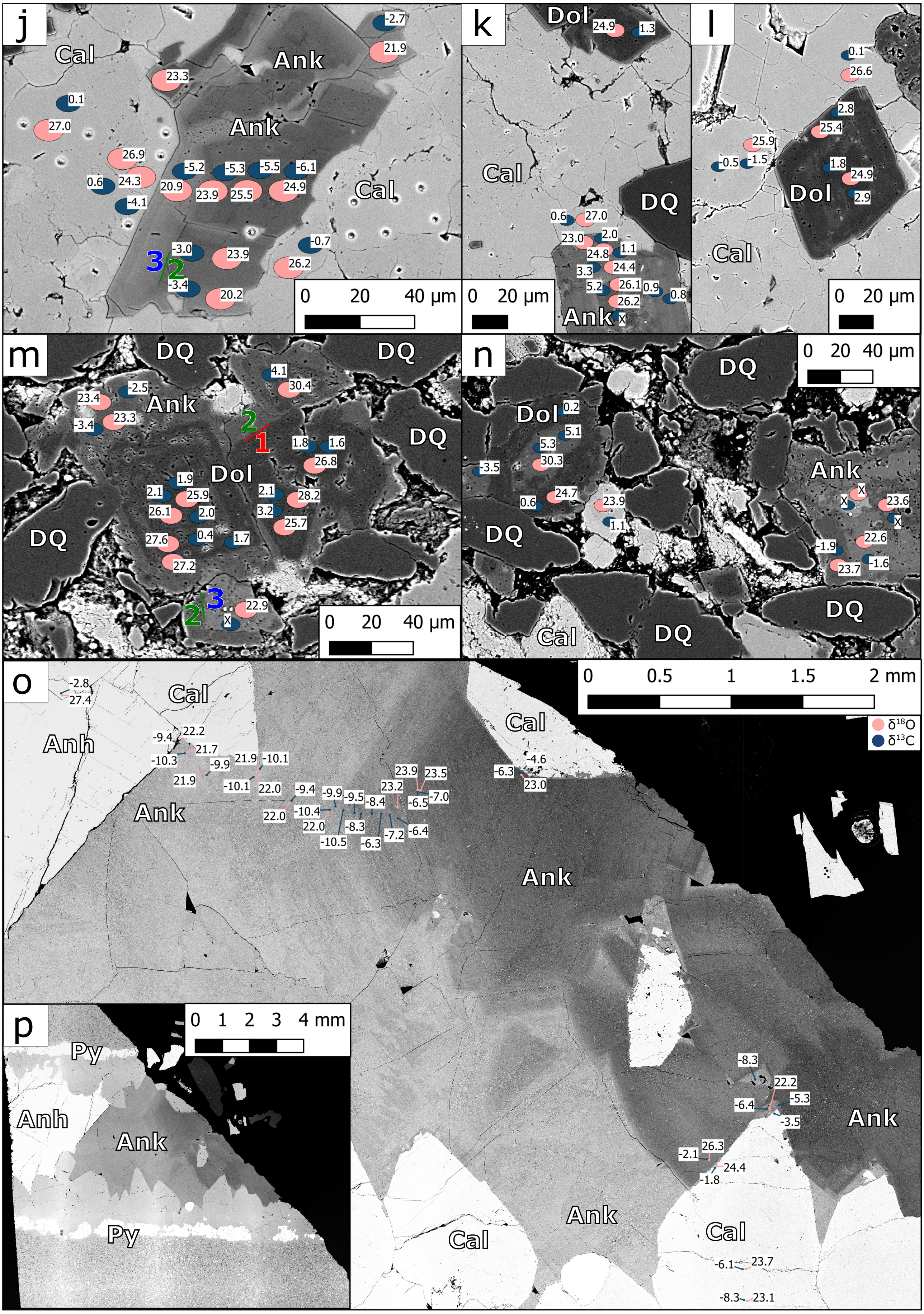
j
Cal
Ank
Ank
Cal
-2.7
21.9
23.3
0.1
27.0
26.9
-5.2
-5.3
-5.5
-6.1
0.6
24.3
20.9
23.9
25.5
24.9
-4.1
-0.7
-3.0
23.9
3/2
26.2
-3.4
20.2
0
20
40 µm
k
Dol
24.9
1.3
Cal
DQ
0.6
27.0
23.0
2.0
24.8
1.1
3.3
24.4
5.2
26.1
0.9
0.8
26.2
Ank
X
0
20 µm
l
0.1
26.6
2.8
25.4
25.9
-0.5
-1.5
1.8
24.9
Dol
2.9
Cal
0
20 µm
m
DQ
DQ
4.1
30.4
-2.5
Ank
23.4
23.3
-3.4
2/1
DQ
1.8
1.6
26.8
Dol
1.9
2.1
25.9
2.1
28.2
26.1
2.0
3.2
25.7
DQ
27.6
0.4
1.7
27.2
2
3
22.9
X
0
20
40 µm
n
0
20
40 µm
DQ
Dol
0.2
5.1
5.3
30.3
-3.5
Ank
24.7
0.6
23.9
X
X
23.6
X
1.1
DQ
22.6
-1.9
-1.6
23.7
DQ
Cal
DQ
o
0
0.5
1
1.5
2 mm
δ18O
δ13C
-2.8
27.4
Cal
Anh
22.2
-9.4
21.7
-10.3
-9.9
21.9
-10.1
21.9
-10.1
22.0
Ank
-9.4
22.0
-10.4
-9.9
22.0
-9.5
-10.5
-8.3
-8.4
-6.3
23.9
23.5
23.2
-6.5
-7.0
-7.2
-6.4
Cal
-4.6
-6.3
23.0
Ank
p
0
1
2
3
4 mm
Py
Anh
Ank
Py
-8.3
22.2
-6.4
-5.3
-3.5
Ank
26.3
-2.1
24.4
-1.8
Ank
Cal
Cal
-6.1
23.7
-8.3
23.1

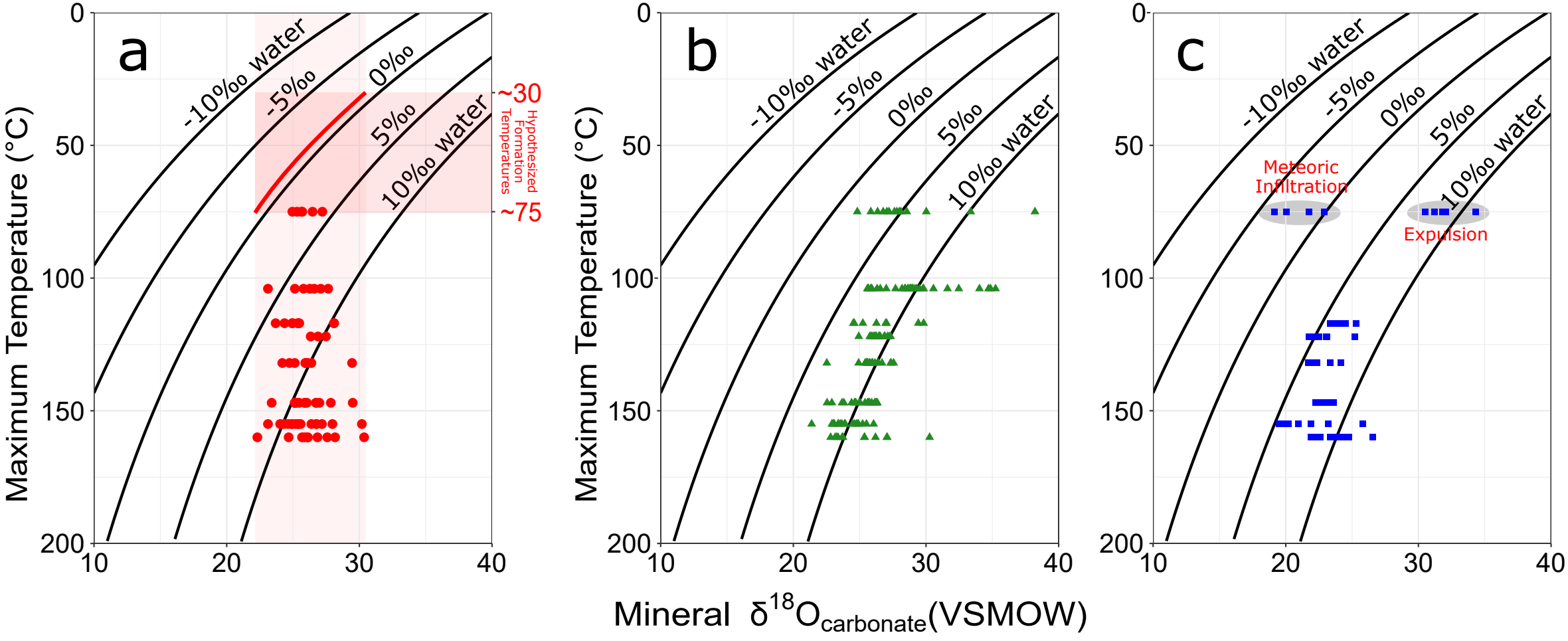
a
b
c
-10‰ water
-5‰
0‰
5‰
10‰ water
Maximum Temperature (°C)
Mineral δ18Ocarbonate(VSMOW)
~30
~75
Hypothesized Formation Temperatures
Meteoric Infiltration
Expulsion
0
50
100
150
200
10
20
30
40

Transect Name	NDGS Well #	API #	Original Operator	Well Name	Latitude
Well 1	24883	33009023020000	CORINTHIAN EXPLORATION (USA) CORP	2-BRENDEN 9-33 1-M	48.9856084
Well 2	20249	33075014170000	MUREX PETROLEUM CORPORATION	HEATHER LYNNE 1	48.8628573
Well 3	17272	33101004730000	HESS CORPORATION	IM-SHORTY-159-88-0805H-1	48.604914
Well 4	17676	33061008840000	EOG RESOURCES, INC.	SIDONIA 1-06H	48.5330324
Well 5	16586	33061005300000	EOG RESOURCES, INC.	BURES 1-17H	48.3405436
Well 6	17015	33105016670000	HEADINGTON OIL COMPANY LLC	NESSON STATE 42X-36	48.2913654
Well 7	21668	33053038190000	BURLINGTON RESOURCES OIL & GAS COMPANY LP	UBERWACHEN 22-34	48.03333
Well 8	12785	33025004470000	MAXUS EXPLORATION CO.	CARUS FEE #21-19	47.542727
Well 9	22493	33053040110000	NEWFIELD PRODUCTION COMPANY	BERNICE 150-99-20-17-2H	47.7914583

Longitude	Depth of SIMS sample (ft from surface)	Depth of SIMS sample (~m from surface)
-100.6472088	3743.4	1141
-101.8269428	6013.4	1833
-102.0619859	7591.5	2314
-102.3443921	8738.4	2663
-102.5459482	9812.5	2991
-102.8284633	10354.4	3156
-102.8861333	10225.8/10233.5	3117/3119
-102.963685	11315.5	3449
-103.3731646	11122.9/11159	3390/3401

FileNo	LATITUDE	LONGITUDE	alt_name
24883	48.98561	-100.647	#1 (24883)
20249	48.86286	-101.827	#2 (20249)
17272	48.60491	-102.062	#3 (17272)
17676	48.53303	-102.344	#4 (17676)
16586	48.34054	-102.546	#5 (16586)
17015	48.29137	-102.828	#6 (17015)
21668	48.03333	-102.886	#7 (21668)
12785	47.54273	-102.964	#8 (12785)
22493	47.79146	-103.373	#9 (22493)
21706	47.81794	-103.172	

API	FileNo	OriginalOp	OriginalWe	CurrentOpe	CurrentWel	FieldName	CountyName
33105016670000	17015	HEADINGTON OIL COMPANY LLC	NESSON STATE 42X-36	XTO ENERGY INC.	NESSON STATE 42X-36	BEAVER LODGE	WILLIAMS
33101004730000	17272	HESS CORPORATION	IM-SHORTY-159-88-0805H-1	HESS BAKKEN INVESTMENTS II, LLC	IM-SHORTY-159-88-0805H-1	WILDCAT	WARD
33075014170000	20249	MUREX PETROLEUM CORPORATION	HEATHER LYNNE 1	MUREX PETROLEUM CORPORATION	HEATHER LYNNE 1	GROVER	RENVILLE
33061008840000	17676	EOG RESOURCES, INC.	SIDONIA 1-06H	EOG RESOURCES, INC.	SIDONIA 1-06H	CLEAR WATER	MOUNTRAIL
33061005300000	16586	EOG RESOURCES, INC.	BURES 1-17H	EOG RESOURCES, INC.	ROSS 7-17H	ALGER	MOUNTRAIL
33053040110000	22493	NEWFIELD PRODUCTION COMPANY	BERNICE 150-99-20-17-2H	NEWFIELD PRODUCTION COMPANY	BERNICE 150-99-20-17-2H	SOUTH TOBACCO GARDEN	MCKENZIE
33053038290000	21706	DENBURY ONSHORE, LLC	LUNDIN 11-13SEH	XTO ENERGY INC.	LUNDIN 11-13SEH	SIVERSTON	MCKENZIE

33053038190000	21668	BURLINGTON RESOURCES OIL & GAS COMPANY LP	UBERWACHEN 22-34	BURLINGTON RESOURCES OIL & GAS COMPANY LP	UBERWACHEN 22-34	CHARLSON	MCKENZIE
33025004470000	12785	MAXUS EXPLORATION CO.	CARUS FEE #21-19	LELAND OIL & GAS, LLC	CARUS FEE 21-19	BIG GULCH	DUNN
33009023020000	24883	CORINTHIAN EXPLORATION (USA) CORP	2-BRENDEN 9-33 1-M	CRESCENT POINT ENERGY U.S. CORP.	2-BRENDEN 9-33 1-M	NORTH SOURIS	BOTTINEAU

Township	Range	Section	QQ	Footages	Hole_Type	LATITUDE	LONGITUDE	FirstSpudD
156	95	36	NESE	2640 FNL 210 FEL	Horizontal	48.29137	-102.828	2/4/08
159	88	8	SESE	210 FSL 455 FEL	Horizontal	48.60491	-102.062	5/7/08
162	86	16	NENE	660 FNL 660 FEL	Verticle	48.86286	-101.827	1/30/11
158	90	6	SESE	433 FSL 425 FEL	Horizontal	48.53303	-102.344	10/19/08
156	92	17	NWNW	400 FNL 400 FWL	Horizontal	48.34054	-102.546	12/8/08
150	99	20	SESE	410 FSL 1170 FEL	Horizontal	47.79146	-103.373	5/22/12
150	98	13	NWNW	300 FNL 945 FWL	Horizontal	47.81794	-103.172	1/16/12

153	95	34	SENW	1761 FNL 1540 FWL	Verticle	48.03333	-102.886	11/25/11
147	96	19	NENW	980 FNL 1785 FWL	Verticle	47.54273	-102.964	6/22/90
164	77	33	NESE	1767 FSL 1066 FEL	Horizontal	48.98561	-100.647	3/1/13

Measured TD	KBElev	DFElev	GRElev	GLElev	TY-BCHR	TY-BCHN	K-P	K-PJRS
14578	2382			2362			1844	
17790	2038			2012			1470	
8950	1805		1785	1786			891	
13992	2313			2287			1912	
14926	2319			2293			2034	
20850	2258		2233	2235			2049	
20897	2179		2155	2160			1990	

10649	2281		2255	2260				
11700	2547							
6080	1623		1609	1609			102	

K-PES	K-NB	K-GH	K-M	K-N	K-IK	J-S	J-R	T-S
		4275	4578	4706	4941	5386	5864	6395
		3564	3863		4205	4523	4891	5441
		2684	2956	2043	3222	3554	3851	4402
		4115	4423		4780	5140	5532	6110
		4402	4740	4850	5090	5478	5884	6485
		4779	5225		5629	5998	6505	7103
		4629	5074		5450	5852	6336	6912

		4000	4388	4504	4755	5195	5651	6182
		4911	5376	5502	5746	6174	6641	7151
		1554	1811		1981	2302		2894

PM-MK	PM-OP	PM-EBA	PM-BC	PN-T	M-EBS	M-BS	M-KL	M-MDUN
	6735	7109		7316	7540		7905	
							5761	
								4623
					6518		6789	
		6976		7091	7297		7600	
7566	7608	7926		8143	8351		8690	
7387	7427	7787		8059	8336		8634	

6559	6589	6920			7450		7790	
7550	7589	7952		8475	8636		8960	
								3016

M-MD	M-MDR	M-MDLS	M-MDFA	M-MDFY	M-MDSA	M-MDTI	M-MDLP	MD-B
8056	8624	8699	8900				9496	10294
5921	6161				6382		6946	7569
					4873	5256	5434	5999
6958	7254	7319	7544				8094	8721
7752	8204	8280	8456				9096	
8835	9443	9540	9759					
8783	9397	9492	9715				10246	

7942	8562	8636	8826				9464	10230
9106	9614	9682	9884				10418	11289
						3024	3097	3710

D-DV	D-TF	D-BB	D-DP	D-SR	D-DB	D-PE	D-W	S-I
	10437							
	7620							
	6029	6217	6324	6766	7080	7251	7732	7875
	8794							

	10321	10530	10620					
	11358	11617						
	3807							

S-CL	O-G	O-ST	O-RR	O-WR	O-WI	O-BI	CO-D	PC
8098	8566	8638	8695					

LogsOnFile	MD_County	MD_CoreTy	MD_CoreFm	MD_Depth	MD_Library	MD_FileNo	MD_APINo	MD_WellLo
AIG,AIG,CBL,CND,DGWD,DTSM,DTSM,MRI,MRI,RST,SOS,SPL	Williams	LS	MD-B	10454-10469	11703	17015ÿ[ViewCore]	3.31E+09	NESE 36-156-95
AIG,CAL,CBL,CND,DTSM,DTSM	Ward	LS	MD-B	7540-7662	28103/203	17272ÿ[ViewCore]	3.31E+09	SESE 8-159-88
CAL,CBL,CND,DTSM,GR,LGR	Renville	LS	MD-B	5980-6040	12102	20249ÿ[ViewCore]	3.31E+09	NENE 16-162-86
AIG,CBL,CBL,CND,DGWD,DTM,DTM,DTSM,DTSM,DTSM,DTSM,GR,GR,SOS	Mountrail	LS	MD-B	8758-8872	8502	17676ÿ[ViewCore]	3.31E+09	SESE 6-158-90
AIG,BCS,CAL,CBL,CND,DTM,DTSM,DTSM,DTSM,DTSM,GR	Mountrail	LS	MD-B	9842-9951	8803	16586ÿ[ViewCore]	3.31E+09	NWNW 17-156-92
AIG,AIG,CAL,CBL,CIL,CND,DL,DTSM,DTSM,ECS,GR,MRI	Mckenzie	LS	MD-B	11096-11150	17903	22493ÿ[ViewCore]	3.31E+09	SESE 20-150-99
AIG,CAL,CBL,CIL,CND,DTSM,DTSM,DTSM,DTSM,FMI,SPL	Mckenzie	LS	MD-B	11141-11169	16403	21706ÿ[ViewCore]	3.31E+09	NWNW 13-150-98

AIG,CAL,CBL,CBUS,CCL,CIL,CND,DSSI,DTM,DTSM,GR,SOS,SPL	Mckenzie	LS	MD-B	10264-10295	16202	21668ÿ[ViewCore]	3.31E+09	SENW 34-153-95
CBL,CND,DS,DTS,PHI	Dunn	TS	MD-B	11261-11361	T-92	12785ÿ[ViewCore]	3.3E+09	NENW 19-147-96
CAL,CBL,CND,DIL,DTSM,DTSM,GWD,SON	Bottineau	LS	MD-B	3725-3786	25602	24883ÿ[ViewCore]	3.3E+09	NESE 33-164-77

MD_Origina	MD_Origi_1	MD_TS	MD_Core	MD_TS_Core	metersMD-B	metersD-TF	Favorite	alt_name
HEADINGTON OIL COMPANY LLC	NESSON STATE 42X-36	FALSE	TRUE	Core	3138	3181	Y	#6 (17015)
HESS CORPORATION	IM-SHORTY-159-88-0805H-1	FALSE	TRUE	Core	2307	2323	Y	#3 (17272)
MUREX PETROLEUM CORPORATION	HEATHER LYNNE 1	FALSE	TRUE	Core	1828	1838	Y	#2 (20249)
EOG RESOURCES, INC.	SIDONIA 1-06H	FALSE	TRUE	Core	2658	2680	Y	#4 (17676)
EOG RESOURCES, INC.	BURES 1-17H	FALSE	TRUE	Core			Y	#5 (16586)
NEWFIELD PRODUCTION COMPANY	BERNICE 150-99-20-17-2H	FALSE	TRUE	Core			Y	#9 (22493)
DENBURY ONSHORE, LLC	LUNDIN 11-13SEH	FALSE	TRUE	Core			YN	

BURLINGTON RESOURCES OIL & GAS COMPANY LP	UBERWACHEN 22-34	FALSE	TRUE	Core	3118	3146	Y	#7 (21668)
MAXUS EXPLORATION CO.	CARUS FEE #21-19	FALSE	TRUE	Core	3441	3462	Y	#8 (12785)
CORINTHIAN EXPLORATION (USA) CORP	2-BRENDEN 9-33 1-M	FALSE	TRUE	Core	1131	1160	Y	#1 (24883)

sulfur	sulfur_lab
Y	17015
N	
N	
N	
Y	16586
N	
Y	21706

N	
Y	12785
N	

Sample	Ankerite-series carbonate		Calc
	δ18O range	δ13C range	δ18O range
Well 1, Sample 24883-3743.4	19.2 to 38.2 (n = 36)	-8.3 to 4.8‰ (n = 31)	20.1 to 29.2 (n = 13)
Well 2, Sample 20249-6013.4	23.1 to 35.2‰ (n=63)	-3.2 to 4.0‰ (n = 40)	27.6 to 29.7‰ (n = 6)
Well 3, Sample 17272-7591.5	23.4 to 29.8‰ (n = 31)	-7.2 to 2.6‰ (n=30)	23.2 to 31.3‰ (n = 10)
Well 4, Sample 17676-8738.4	21.8 to 28.5‰ (n = 32)	-8.8 to 1.4 (n = 37)	24.5 to 32.1‰ (n = 15)
Well 5, Sample 16586-9812.5	21.7 to 29.5‰ (n = 32)	-5.9 to 3.3‰ (n = 39)	24.5 to 28.0 (n = 7)
Well 6, Sample 17015-10354.4	22.3 to 29.5‰ (n = 47)	-5.5 to 5.1‰ (n = 51)	22.7 to 25.3‰ (n = 17)
Well 7, Sample 21668-10225.8	19.3 to 27.7‰ (n = 11)	-8.3 to -0.2‰ (n = 15)	20.4 to 30.8‰ (n = 9)
Well 7, Sample 21668-10233.5	22.4 to 30.0‰ (n = 19)	-4.6. to 2.5‰ (n = 16)	26.4 to 28.1 (n = 4)
Well 8, Sample 12785-11315.5	20.2 to 27.2‰ (n = 20)	-6.1 to 5.2‰ (n = 21)	22.9 to 27.0‰ (n=18)
Well 9, Sample 22493-11122.9	22.3 to 30.4‰ (n = 34)	-5.6 to 5.3‰ (n = 37)	24.0 to 24.6‰ (n = 3)
Well 9, Sample 22493-11159	21.9 to 26.6 ‰ (n = 15)	-10.3 to -1.8‰ (n = 25)	23.1 to 29.5‰ (n = 15)

ite
δ13C range
-7.4 to 2.6 (n = 13)
-0.7 to 0.8‰ (n = 5)
-4.2 to 5.7‰ (n = 11)
-10.3 to 4.8‰ (n = 17)
-2.0 to 5.2‰ (n = 10)
-2.2 to 7.5‰ (n = 17)
-6.3 to 6.1‰ (n = 9)
-0.7 to 5.5‰ (n = 4)
-4.1 to 5.9‰ (n=19)
-2.1 to 1.1‰ (n = 2)
-17.4 to -1.8‰ (n = 20)